AUTOMATIC CONTROL OF PROPELLER PITCH

by

LIEUTENANT DAVID B. FLANAGAN

U.S. COAST GUARD

SUBMITTED IN PARTIAL FULFILLMENT OF THE
REQUIREMENTS FOR THE DEGREE OF NAVAL ENGINEER
and
FOR THE DEGREE OF MASTER OF SCIENCE IN
NAVAL ARCHITECTURE AND MARINE ENGINEERING
at the
MASSACHUSETTS INSTITUTE OF TECHNOLOGY
20 May 1962

Thesis Supervisor: S. Curtis Powell, DOTT. ING.
Title: Associate Professor of Marine Engineering

AUTOMATIC CONTROL OF PROPELLER PITCH

by

DAVID B. FLANAGAN, U.S. COAST GUARD

B.S., U.S. COAST GUARD ACADEMY

(1955)

SUBMITTED IN PARTIAL FULFILLMENT OF THE

REQUIREMENTS FOR THE DEGREES OF NAVAL ENGINEER

and

MASTER OF SCIENCE

IN NAVAL ARCHITECTURE AND MARINE ENGINEERING

at the

MASSACHUSETTS INSTITUTE OF TECHNOLOGY

June, 1962

AUTOMATIC CONTROL OF PROPELLER PITCH, by DAVID B. FLANAGAN. Submitted to the Department of Naval Architecture and Marine Engineering on 19 May 1962 in partial fulfillment of the requirements for the degree of Naval Engineer and the degree of Master of Science in Naval Architecture and Marine Engineering.

ABSTRACT

The object of this study was to determine the feasibility of automatically controlling propeller pitch to reduce RPM fluctuations caused by variations in propeller speed of advance. The investigation was made ignoring the reduced frequency effect and power plant governing.

A Victory Ship (AP2) was chosen as a prototype and a feedback system controlling the pitch of a controllable pitch propeller was developed. A non-linear analogue computer program approximating the system and the propeller characteristics is presented. Electronic difficulties prevented obtaining total system response from this program. The computer study indicated that a linear analysis would be useful.

The linear analysis indicated that, for the prototype, in order to achieve a reduction in RPM fluctuation of 10% of that present in the fixed pitch case, a hydralic pump consuming over 300 HP would be needed. Systems utilizing RPM, shaft torque, and thrust are analyzed. Thrust sensing provided the poorest response and in fact increased the RPM fluctuation for lower frequencies.

RPM governing by automatic control of propeller pitch was found to be inadvisable unless major design changes are made to reduce the spindle torque of presently available controllable pitch propellers.

Thesis Supervisor: S. Curtis Powell

Title: Associate Professor of Marine Engineering

TABLE OF CONTENTS

LIST OF FIGURES

LIST OF FIGURES (cont'd)

LIST OF TABLES

LIST OF SYMBOLS

a,b,c,d,e,f	= mechanical linkage lengths, ft.
b	= spindle bearing length, ft.
h_i	= vertical intercept on the linearized propeller curve i.
k	= spring constant, lb/ft.
ℓ	= distance from center of hydrodynamic pressure on a blade to the center of the spindle axis bearing, ft.
m_i	= slope of linearized propeller curve
n	= propeller rotational speed, rev. per second.
p	= propeller pitch, ft.
r	= spindle bearing radius, ft.
S	= complex frequency of Laplace Transform, sec^{-1}
t	= blade thickness, ft.
w	= wake fraction
x	= mechanical input to the variable displacement pump, in.
x_c	= control rod displacement, in.
y	= mechanical input to pitch control mechanism
A_R	= area of piston, in^2
C	= initial displacement of safety spring, ft.
D	= propeller diameter, ft.

F_c = control rod force, lb.

F_{cQ} = blade torque component of control rod force

G_i = gain for system using i^{th} sensing method.

I = area moment of inertia, ft^4

J = advance coefficient, $\frac{V_o}{nD}$

J_{iE}' = polar mass moment of inertia referred to the propeller shaft, lb-ft-sec^2

J_{iP}' = polar mass moment of inertia of the propeller and entrained water

K_i = constant, used in non-linear analysis

K_i^* = constant, used in linear analysis

K_P = pump constant, $\frac{in^3}{sec\text{-}in}$

K_L = leakage constant, $\frac{in^5}{lb}$

K_C = compliance constant, in/lb

M = mechanical feedback constant

$$= \frac{12G_2eRK_P}{(e+f_\ell)\pi D}$$

M_c = mass of control rod, $\frac{lb\text{-}sec}{ft}$

N = number of propeller blades

Q_E = engine torque, lb-ft

Q_P = propeller torque, lb-ft

Q_S = shaft torque, lb-ft

R = hub mechanism crank length, ft.

T = propeller thrust, lb

$T_\perp$ = thrust perpendicular to the blade spindle axis, lb

V	= ship speed, knots
V_o	= speed of advance, ft/sec
ΔV_o	= sinusoidal amplitude of fluctuation in speed of advance
X,Y	= coordinates of ellipse, ft.
$\mathcal{L}_B$	= blade damping, lb-ft-sec/rad
$\mathcal{L}_E$	= engine damping, lb-ft-sec/rad
$\mathcal{L}_P$	= propeller damping, lb-ft-sec/rad
$\mathcal{N}$	= piston damping, lb-sec/ft
ζ	= damping coefficient of second order polynomial in S.
ω	= shaft angular speed, rad/sec

Dotted variables correspond to derivatives.

Primed variables denote incremental quantities.

ACKNOWLEDGMENTS

The author wishes to express gratitude to the following for their assistance and encouragement:

Professor S. Curtis Powell of the Department of Naval Architecture and Marine Engineering, his thesis supervisor.

Professor Walter McKay of the Department of Aeronautics and Astronautics, his thesis advisor.

I.

INTRODUCTION

The propulsion systems of ships operating in a seaway undergo speed fluctuations caused by variations in propeller load. The shaft torque produced by the propeller is a function of the flow velocity across the propeller disc area. As the ship rolls, pitches, and encounters waves this flow velocity fluctuates causing a fluctuation in shaft torque which the propulsion system must overcome. The propulsion system responds to the fluctuating load by allowing fluctuations in RPM. The amount of RPM fluctuation present depends on the system inertia, damping, and the effectiveness of the governing, if provided, of the power plant. High speed turbine installations with large reduction gears experience less RPM fluctuation difficulties than do direct drive diesels.*

The largest variation of flow velocity averaged over the propeller disc area, henceforth called speed of advance, will probably occur at resonant pitching. Model tests

---

* Evans, Harvey J. Conversations before seminar group of Department of Naval Architecture and Marine Engineering, M.I.T. 24 April 1962.

indicate that at this condition the variation of speed of advance could be as high as 0.43 of the steady state value.** For a geared turbine ship such as the Victory Ship (AP2) with a fixed pitch propeller a fluctuation of about 6 RPM will result at the frequency of resonant pitching, which is about 0.03 cycles per second. Calculations leading to these figures are given in Appendix E. For systems with less effective inertia and damping the fluctuations would be correspondingly higher.

Ship's propellers are designed to operate efficiently at a designed speed of advance. Their efficiency is reduced when subjected to a constantly varying speed of advance. The propulsion system could deliver full power when the ship was operating in a seaway if the load could be made sufficiently constant.

A controllable pitch propeller has the ability to alter the propeller pitch at any time. If the pitch were altered to counteract the effect of the changing speed of advance, a constant torque load would be provided to the power plant. The efficiency of the power plant and propeller might be increased and the entire system could

---

** Burtis, Evenson M. and J.D. O'Connell. Measurement of Ship Model Wake Variation in Rough Water, Naval Engineers Thesis, Department of Naval Architecture and Marine Engineering, M.I.T. Cambridge, 1959.

be operated in heavy seas at high power. A literature survey has revealed that no reported investigation of this possibility has been made. Extensive use of one governor systems controlling RPM by altering both pitch and throttle setting has been made by the aircraft industry in conjunction with turboprop aircraft.

The purpose of this paper was to investigate the possibility of governing propulsion system RPM by automatic control of propeller pitch. Systems sensing RPM, torque, and propeller thrust were investigated. System speed governing by controlling the load may or may not be more advantageous than conventional governing of the power plant. The regulation of some variable other than speed might also provide a more optimum overall operation. This investigation, however, examines the feasibility of speed governing through propeller load control only.

II.

GENERAL PROCEDURE

Several major analytical assumptions were made at the outset. Unsteady flow was treated using the quasi-steady approximation and the reduced frequency effects were neglected. The speed of advance was assumed to be a steady state value with a sinusoidal fluctuation superimposed thereon. The control systems investigated contained a simple one loop feedback with no special compensating networks. The power plant was assumed to deliver constant torque and no model of the governor was developed.

The standard method of presenting propeller characteristics envolves a plot of non-dimensional thrust and torque coefficients as functions of advance ratio, J, and pitch ratio $\frac{p}{D}$. These plots are very nearly families of straight lines. For the non-linear study the propeller curves were assumed to be families of straight lines. The slopes and values of the actual and the assumed curves are the same at the operating point. The accuracy of the approximation decreases as conditions depart from the operating point. The approximations lead to expressions (6) and (13)

for propeller torque and thrust respectively as derived in Appendix A.

$$Q_P = K_1 p\omega^2 - K_2 V_o \omega - K_3 \omega^2 \quad . \quad (6)$$

$$T = K_4 p\omega^2 - K_5 V_o \omega - K_6 \omega^2 \quad . \quad (13)$$

The K's are constants for a given propeller and depend on both the propeller curves and the dimensions of the propeller.

For the linear analysis, the propeller torque and thrust were assumed to be linear functions of speed of advance, pitch, and RPM. This is the customary incremental linear analysis and is valid only for small variations of the variables about the operating point. The equations for incremental variations in propeller torque and thrust are derived in Appendix E and are

$$Q_P' = K_1^* V_o' + K^* p' + K^* \omega' \quad (81)$$

and

$$T = K^* V_o' + K^* p' + K^* \omega' \quad . \quad (100)$$

The K^*'s are found by assuming a small change in the corresponding variable ($\pm$ 0.1), and while keeping all other independent variables constant, determining from the propeller curves the corresponding change in the dependent variable. The K^* then becomes the dependent variable change divided by 0.2 The Troost Standard Series for Single Screw Merchant Vessels (B4-55)

propeller curves were used throughout.*

No test data providing blade spindle torque directly is available. The torque about the blade spindle axis was assumed to be composed of hydrodynamic, sliding friction, viscous friction, inertia, and centrifugal force components. As with the propeller torque and thrust coefficients, the hydrodynamic component of blade torque can be represented by a family of blade torque coefficient curves, K_B, where advance ratio and pitch ratio are the independent variables. These curves were also assumed to be families of straight lines and the resulting expression for hydrodynamic blade torque as derived in Appendix A is

$$Q_{BH} = K_7 p\omega^2 - K_8 V_o \omega - K_9 \omega^2 \quad . \qquad (21)$$

Reference (11) contains data on the control rod forces for a controllable pitch propeller installation on a tug, (YTB-502), while underway at various speeds. This data also includes details of the pitch setting mechanism, ship's speed, centrifugal force components as functions of RPM and pitch, and other useful information. An approximate wake fraction of 0.164 was assumed based on the block coefficient of the tug. Since the tests were

---

* Lewis, F.M. "Propeller Coefficients and the Powering of Ships," Society of Naval Architects and Marine Engineers Paper, Nov. 1951.

made under steady conditions, the only forces assumed acting were hydrodynamic and centrifugal. After subtracting the centrifugal component, the control rod force was converted to a spindle torque, non-dimensionalized, and finally plotted as blade torque coefficient versus advance ratio and pitch ratio. The results are shown in Figure B-3 below and the calculations leading to this plot are given in Appendix B.

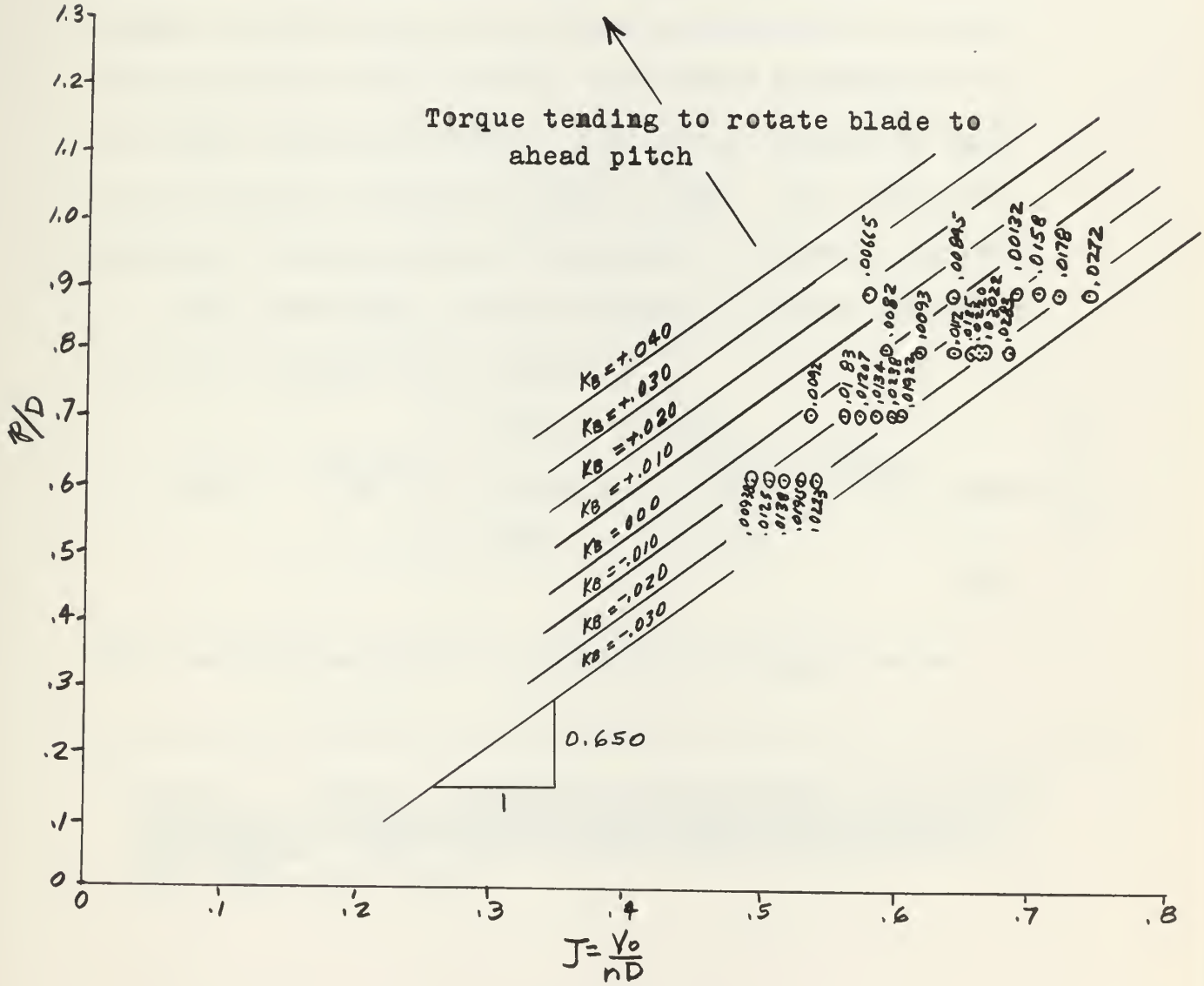

FIGURE B-3

Derived K_B Curves for YTB-502

As before stated, the K_B curves were assumed linear. The hydrodynamic spindle torque is a strong function of the location of the spindle axis relative to the hydrodynamic center of pressure. It was assumed that the effect of moving the spindle axis would be to shift the K_B values up or down the family of K_B curves. Once the operating point of the prototype assumed for this study was chosen, the operating point of the K_B curves given in Figure B-3 was assumed moved to the prototypes simply by shifting the K_B values corresponding to the tugs operating point to the approximate position of the prototype operating point. This can be justified only in that such a propeller could be made. The slope and spacing of the K_B curves was assumed to remain the same.

The centrifugal force component of blade torque as derived by Boswell and others is*

$$Q_{BC} = -\rho_p \omega^2 N \left[\int_{Hub}^{tip} A_{xy} dr + \int_{root}^{tip} \frac{(I_{max} - I_{min})}{2} \sin 2\alpha \, dr \right]. \quad (28)$$

This expression would be difficult to compute on an

---

* Robert J. Boswell, A Method of Calculating the Spindle Torque of a Controllable-Pitch Propeller at Design Conditions. David Taylor Model Basis Report No. 1529, Aug. 1961, pp. 31-34.

analogue computer and a simplification given in Appendix A leads to expression (35) where the constants K_{10} and K_{11} are functions of propeller geometry alone.

$$Q_{BC} \doteq - K_{10}\omega^2 - K_{11}\omega^2 p \ . \qquad (35)$$

The sliding friction component of spindle torque was obtained from altering the usual expression for sliding friction in a journal bearing to allow for a moment tending to rotate the spindle shaft about a line perpendicular to the shaft centerline. The resulting expression is

$$Q_{BS} = \pm \frac{frT_{\downarrow} \ell \ N}{b} \qquad (38)$$

The double sign in expression (38) indicates that the direction of the torque must be taken either (+) or (-) depending on whether the direction of pitch change is toward lower or higher ahead pitch respectively.

The remaining components of blade spindle torque are obtained by direct application of their respective definitions. The final expression for blade torque is

$$Q_B = \overbrace{K_7 p\omega^2 - K_8 V_o \omega - K_9 \omega^2}^{\text{hydrodynamic}}$$

$$\overbrace{\pm \frac{frT_{\downarrow} \ell \ N}{b}}^{\text{sliding friction}} + \overbrace{\mathcal{L}_B \omega_B N}^{\text{viscous friction}}$$

$$+ \overbrace{J_{iB}' \dot{\omega}_B N}^{\text{inertia}} - \overbrace{K_{10}\omega^2 - K_{11}\omega^2 p}^{\text{centrifugal}} \qquad (38)$$

There are numerous variations of hub mechanisms in use. All are required to convert motion in the direction of the propeller shaft axis into rotation of the blades about their spindle axes. As shown in Appendix A, each of the four mechanisms most frequently used result in approximately the same amount of blade rotation for the same input of linear motion along the propeller axis up to a pitch ratio of 1.5. The same is true for the force-to-torque transmission. For this reason the simplest mathematical relation of the four was used throughout. The results are approximately applicable to all the mechanisms. The expressions used are as follows:

$$\frac{p}{\pi D} = \frac{x_c}{R} \qquad (39)$$

and

$$F_{CQ} = \frac{1}{R} \; Q_B \quad . \qquad (41)$$

There are two general types of controllable pitch propeller mechanisms. The first, designated herein as Design I, utilizes a control rod extending through the propeller shaft and is driven by a hydralic piston within the ship. The second, designated herein as Design II, is driven by a power piston housed within the propeller hub. The power piston of Design II receives oil from a pump within the ship through oil passages in the propeller shaft. Design II, as presently available, includes a safety spring within the hub that makes the

propeller "Fail-safe" by forcing the blades into ahead full pitch in the event of a failure in hydralic oil pressure.

The equation of motion of both these designs is obtained by equating the oil flow from the pump with the sum of the flows into the mechanism which include flow from piston motion, flow from leakage, and flow due to compression of the fluid and expansion of piping. The final equation of both systems are of the same form with the exception of additional terms in the Design II expression that are generated by a safety spring force. Design I was used for all further study. Schematics of both designs are given as Figures A-7 and A-8 in Appendix A. The equation of motion of Design I as derived in Appendix A is

Input Ram Flow Leakage flow

$$K_p x = \dot{p}\ \frac{12RA_R}{D} + \frac{K_L}{A_R}\left[\ \frac{K_7 p\,\omega^2}{R} - \frac{K_8 V_o \omega}{R}\right.$$

$$- \frac{K_9 \omega^2}{R} \pm \left(f_R + \frac{f r T_1 \ell\ N}{bR}\right) + \frac{\dot{p}}{\pi D}\left(\frac{\alpha_B N}{R} + \mathcal{N}_R R\right)$$

$$\left. + \frac{\ddot{p}}{\pi D}\left(\frac{J_{iB} N}{R} + M_c R\right) - \frac{K_{10}\omega^2}{R} - \frac{K_{11}\omega^2 p}{R}\ \right]$$

Compliance Flow

$$+ \frac{K_c}{A_R}\left\{\ \frac{d}{dt}\left[\left(\ \frac{K_7 p\,\omega^2}{R} - \frac{K_8 V_o \omega}{R} - \frac{K_9 \omega^2}{R}\ \right)\right.\right.$$

$$\pm \left(f_R + \frac{frT_1 \ell N}{bR}\right) - \frac{K_{10}\omega^2}{R} - \frac{K_{11}\omega^2 p}{R}\Bigg]$$

$$+ \frac{\ddot{p}}{D}\left(\frac{\mathcal{L}_B N}{R} + \nu_R R\right) + \frac{\ddot{p}}{\pi D}\left(\frac{J i_b' N}{R} + M_c R\right)\Bigg\} \qquad (42)$$

The Victory Ship (AP2) was chosen as a prototype to determine values of the various parameters. This is a 6000 HP geared turbine merchant ship for which considerable data was available. The detailed determination of the various parameters present in equation (42) above is carried out in Appendix B. The propeller blade was assumed to be an elliptical flat plate for the determination of blade inertia and centrifugal force components of blade spindle torque. The dimensions of the hub were obtained by scaling up the design given by Rupp in Reference 11.

The three remaining parameters to fix were area of the ram, the size of the pump, and the hydralic pressure. Since the initial cost and maintenance on systems using more than 1000 psi would be high, this value was chosen as the maximum hydralic pressure. The maximum diameter of power piston that could be accommodated within the propeller hub has a radius of 15.75 inches.

Although Design I has the power piston within the ship, this was assumed the largest piston size that would be fitted. Calculations given in Appendix B show that with the assumed hydralic pressure of 1000 psi and this ram area there is still

a likelihood of stalling the mechanism (by opening relief valves) even with this large size power piston. The maximum combinations of blade centrifugal, hydrodynamic, and sliding friction when acting together require 1000 in^2 of piston area. The assumed piston area is 775 in^2. Larger piston sizes would require larger pump capacities which are excessive for this piston area.

As shown in Appendix E, the time constant of the pitch control mechanism is

$$\tau_P = \frac{RA_R}{K_P \pi D M} \quad . \qquad (60)$$

The effectiveness of the system in regulating RPM fluctuations requires that this time constant be small. The larger pump capacities correspond to larger K_P. Assuming that the marine industry would not accept a device consuming more than 5% of the installed main plant horsepower, a maximum pump size of 300 HP was assumed. K_P was then determined from manufacturers data.

The viscous friction forces were obtained from an analysis of transient spin test data taken by Rupp. This data consists of a plot of control rod forces versus pitch for the operating conditions of going from full ahead to full astern and vice-versa. This data is reproduced as Figure B-7 below. The thrust forces causing high values of sliding friction were assumed zero for this test. The

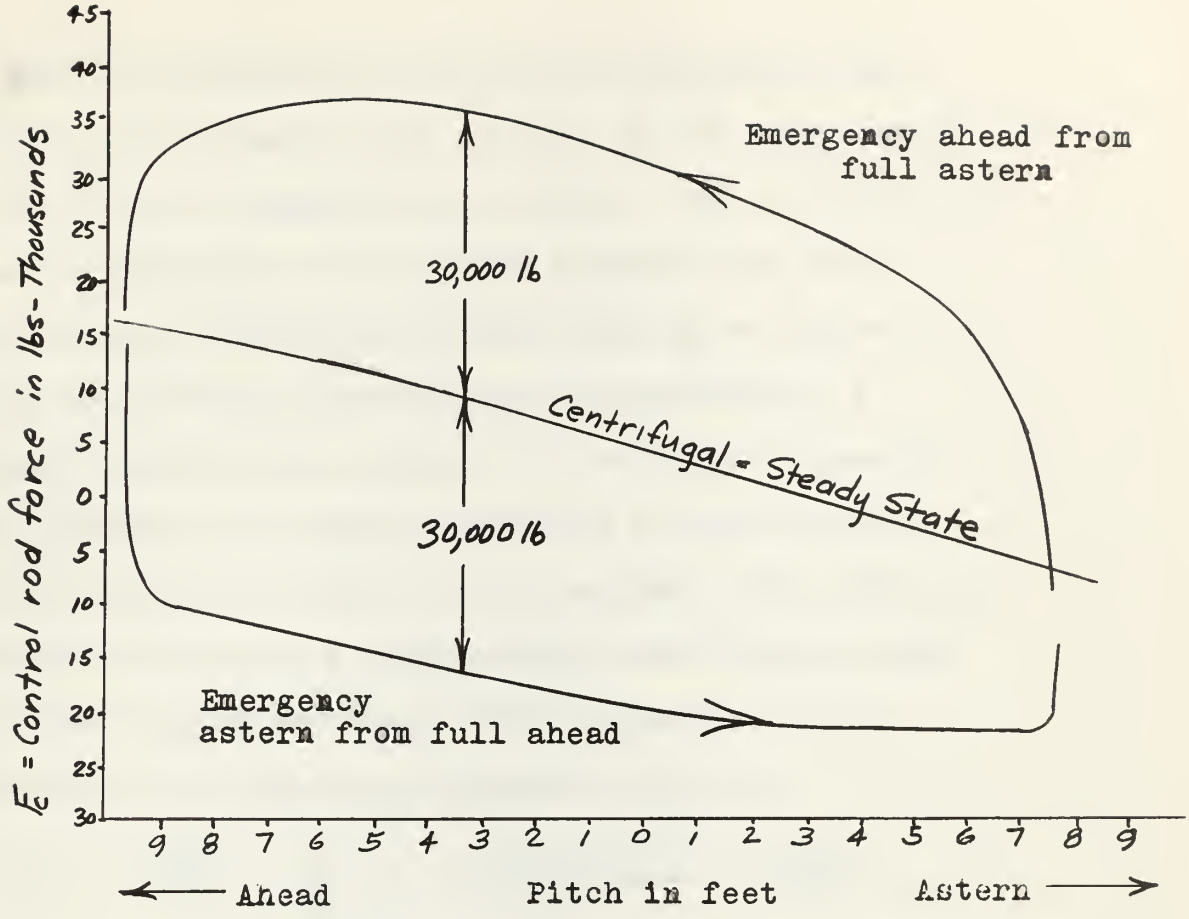

FIGURE B-7

YTB-502 Control Rod Force for Spin Test
in Air From Data by Rupp

long region of both transient curves that are parallel to the steady state condition are assumed to correspond to the condition of maximum pump output and constant piston speed. The deviation from the steady state curve in both cases is approximately 3×10^4 lbs. This control rod force was converted to spindle torque and scaled up by the ratio of propeller diameter squared since viscous friction is proportional to surface area. The speed of rotation was assumed constant and equal to the total angle divided by total time.

The substitution of the various parameters into equation (42) revealed that several of the terms would be very small in comparison to others. The coefficients of each independent variable was examined and those terms having coefficients of less than 1% of those remaining for the same variable were eliminated. A further simplification was made by setting to zero all terms including the first derivative of shaft speed. This assumption is based on the knowledge that propeller RPM does not vary to a large extent even without regulation and should vary less with regulation. The resulting simplification of equation (46) is

$$K_p x = \dot{p}\,\frac{RA_R}{\pi D} + \frac{K_L}{A_R}\left[\frac{(K_7-K_{11})P\omega^2}{R} - \frac{K_8 V_o \omega}{R}\right.$$

$$\left. - \frac{(K_9+K_{10})\omega^2}{R} \pm \left(f_R + \frac{f_r T_\perp \ell\, N}{bR}\right)\right]$$

$$+ \frac{K_C}{A_R}\left[-\frac{K_8 \omega \dot{V}_o}{R} + \frac{\dot{p}}{\pi D}\left(\frac{\mathcal{L}_B N}{R} + \mu_R R\right)\right] \qquad (65)$$

III.

PROCEDURE AND RESULTS OF THE NON-LINEAR ANALOGUE COMPUTER STUDY

A. Procedure

Equations (6), (13), and (65) given above envolve non-linearities in the form of products of independent variables and a discontinuous sliding friction term. If saturation of the pump is also allowed, another discontinuity is introduced which would limit the value of pump output, $k_p x$, to some finite value. All of these non-linearities can be programed on the analogue computer that was available. The program includes four multipliers to generate ω^2, $p\omega^2$, $\sqrt{o}\omega$ and $\hat{V}_o\omega$. It also includes a switching mechanism controlled by the derivative of pitch to approximate sliding friction.

The program was arranged so that shaft torque and thrust were generated in order to test the final system sensing these variables.

The program is shown in Figure C-2 below. The parameters determined in Appendix B were then inserted into the program and voltage scales were assumed for each variable. The gains of various loops were then adjusted

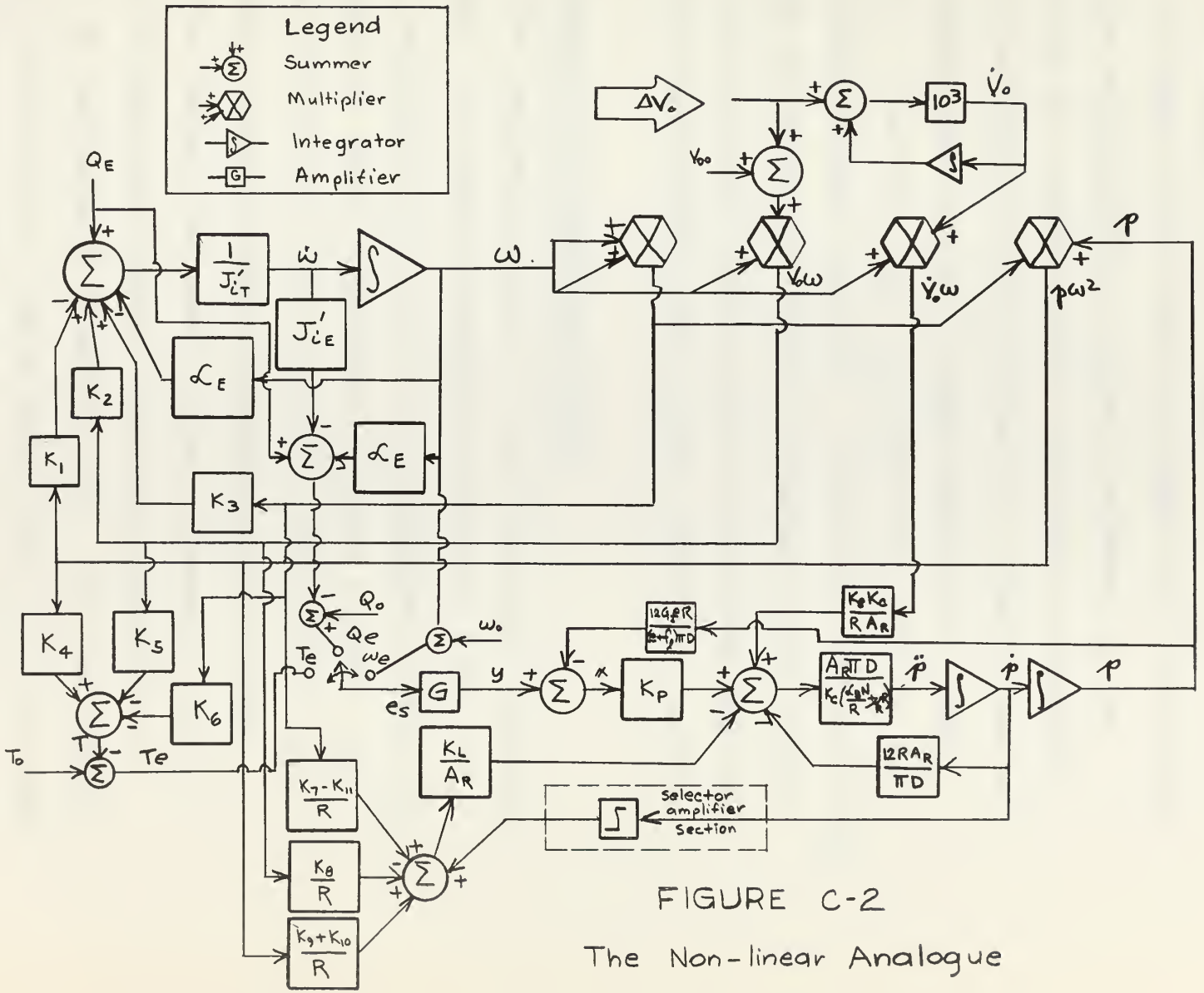

FIGURE C-2

The Non-linear Analogue

to provide signals that would not saturate the various amplifiers and multipliers of the computer. The details of this scaling is given in Appendix C.

The input to the system was taken to be the voltage analogue corresponding to speed of advance, V_o, and consisted of a steady positive value with a sinusoidal voltage of amplitude ΔV_o provided by a signal generator. The output consisted of a voltage analogue for shaft speed, ω , and both input and output were recorded on a two channel Sanborn recorder. It was hoped that data over a range of frequencies could be obtained in this manner for the fixed pitch case as well as the system operating in closed loop sensing shaft speed, torque, and thrust.

B. Results of the Non-Linear Study

The frequency response of the fixed pitch system was obtained. The data is recorded in Appendix C and is shown graphically as a plot of the magnitude of the ratio of output to input in decilogs in Figure I below. The strong stabilizing effect of sliding friction was very apparent. When the signal corresponding to sliding friction feedback was removed with a sinusoidal ΔV_o input of amplitude 6 ft/sec the second derivative of pitch, $\ddot{p}$, increased by a factor of 80. The feed forward path containing $\dot{V}_o\omega$ had no effect on $\ddot{p}$ even for very large values of ΔV_o.

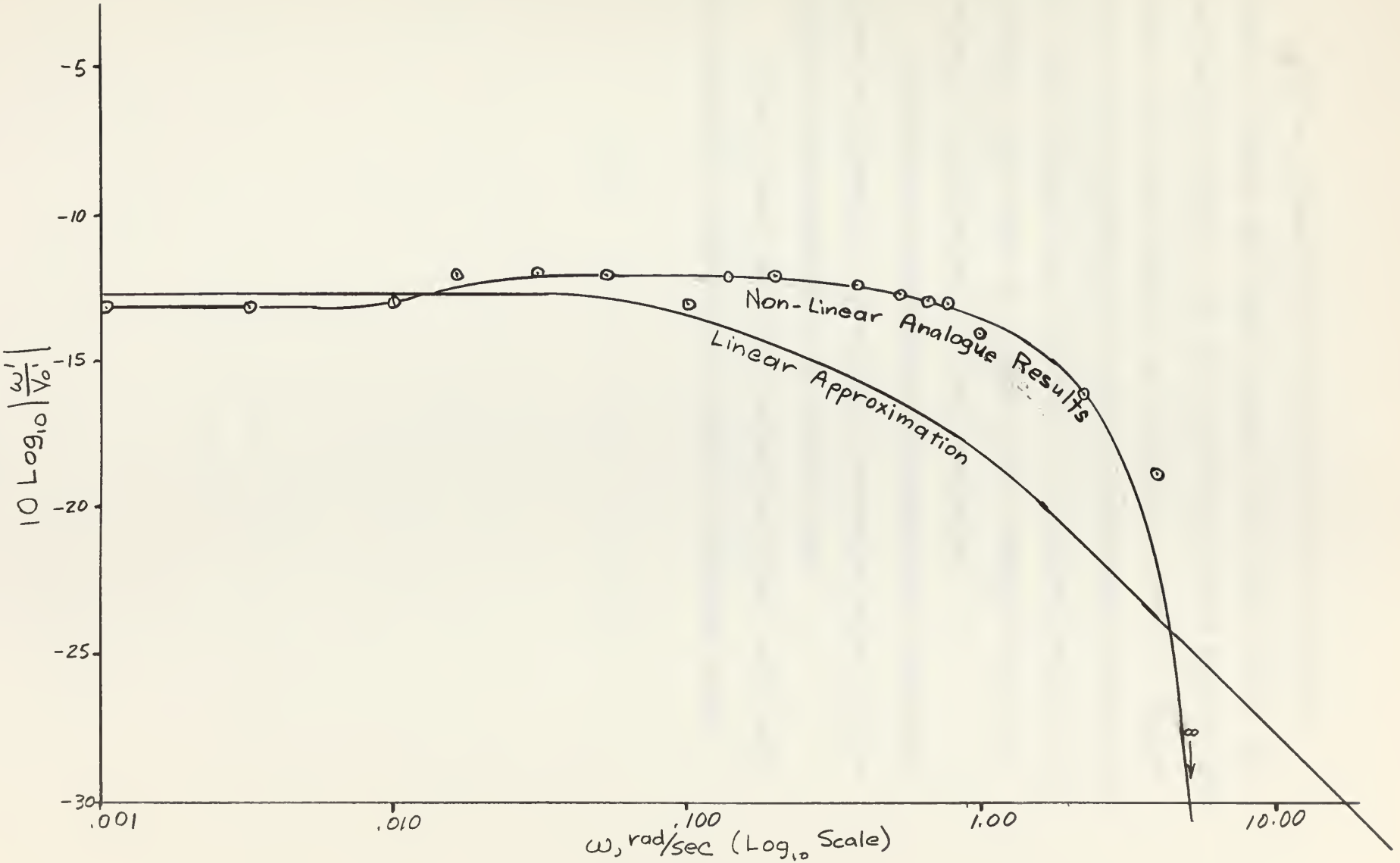

FIGURE I

Fixed Pitch Frequency Response

Values generated by the computer for propeller torque, thrust, and blade torque were within 5% of the calculated values. The time constant of the system with fixed pitch was observed by injecting a step in engine torque and recording the decay in shaft speed variation. The time constant was observed to be approximately 3.28 seconds. The decay to steady state required about 10 seconds (approximately 3 time constants).

Electronic difficulties, the details of which are given in Appendix D, prohibited obtaining data for the control system operating in closed loop.

In all cases the node containing $\ddot{p}$ was very small and consisted primarily of computer generated noise.

IV.

PROCEDURE AND RESULTS OF THE LINEAR STUDY

A. Procedure

The results of the non-linear study indicated that valid further simplifications could be made in equation (46). Eliminating the terms containing $\dot{V}\omega$ and $\ddot{p}$ as suggested by Chapter III above, equation (46) reduces to

$$\dot{p} = \frac{1}{\frac{RA_R}{\pi D}} \left\{ K_P x - \frac{K_L}{A_R} \left[(K_7 - K_{11}) \frac{p\omega^2}{R} \right. \right. \qquad (67)$$

$$\left. \left. - \frac{K_8 V_o \omega}{R} - (K_9 + K_{10}) \frac{\omega^2}{R} \mp \left(f_R + \frac{f_r T_\perp \ell \ N}{bR} \right) \right] \right\}$$

Equation (67) includes ram flow and leakage terms only. Since the linear analysis is valid only for small variations around the operating point, the leakage was assumed constant and is equivalent to an effective reduction in pump output $K_P \not\propto$. As shown in Appendix E, equation (67) eventually reduces to a formula whose frequency domain transfer function is

$$\frac{p'(s)}{y'(s)} = \frac{G/M}{\tau_P S + 1}$$

where $y'(s)$ = Laplace transform of the incremental

mechanical input to the pitch control mechanism.

Using the linear approximations for propeller response before mentioned, and assuming the power plant-propeller system to be a first order system containing inertia and damping, the complete systems for sensing RPM, torque, and thrust were drawn in block diagram form as shown in Figure II.

The gains G_ω and G_Q for the shaft speed and shaft torque sensing systems respectively were chosen so that a damping ratio of 0.4 was assumed by the closed loop system. Higher values of loop gain reduce the low frequency response but cause higher peaking or amplification at a higher frequency. This peaking is apparent at about 2 radians per second as shown in Figure E-6. The gain for thrust, G_T, was taken to be a very low value only to demonstrate that any positive value of G_T is not beneficial in regulating RPM at the lower frequencies.

B. Results

System gain is defined as the ratio of shaft speed variation for a given variation in speed of advance, $\frac{\omega'}{V_o'}$. The system gain for each of the three linear systems pictured in Figure II was obtained and plotted by the standard methods.

The results are shown in Figure E-6 where system gain is plotted in decilogs.

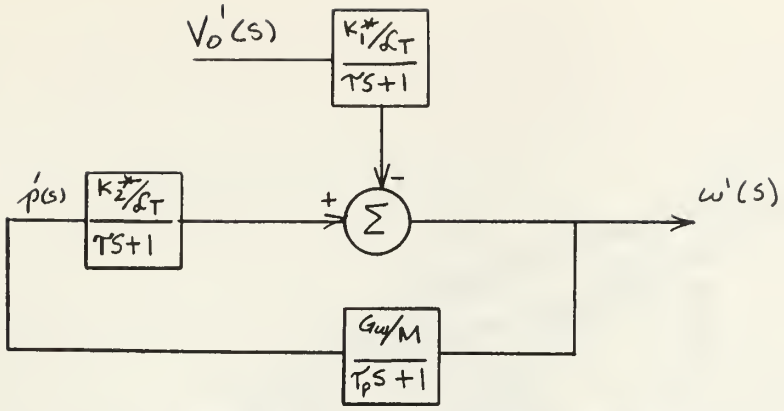

(a) Regulation by Shaft Speed Sensing

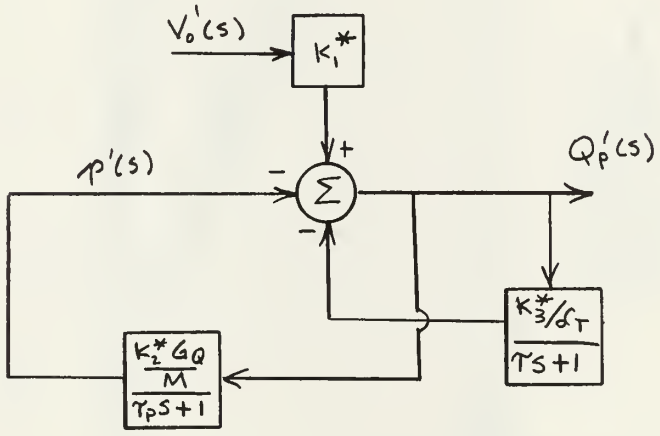

(b) Regulation by Shaft Torque Sensing

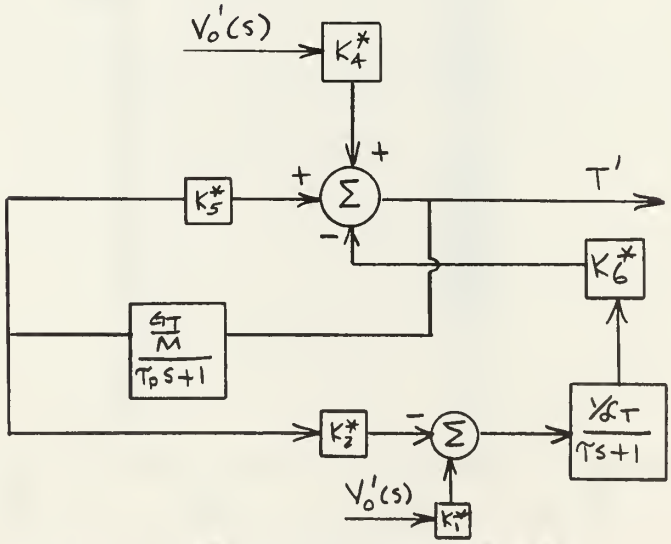

(c) Regulation by Thrust Sensing

FIGURE II

Linear Approximation to Complete Systems

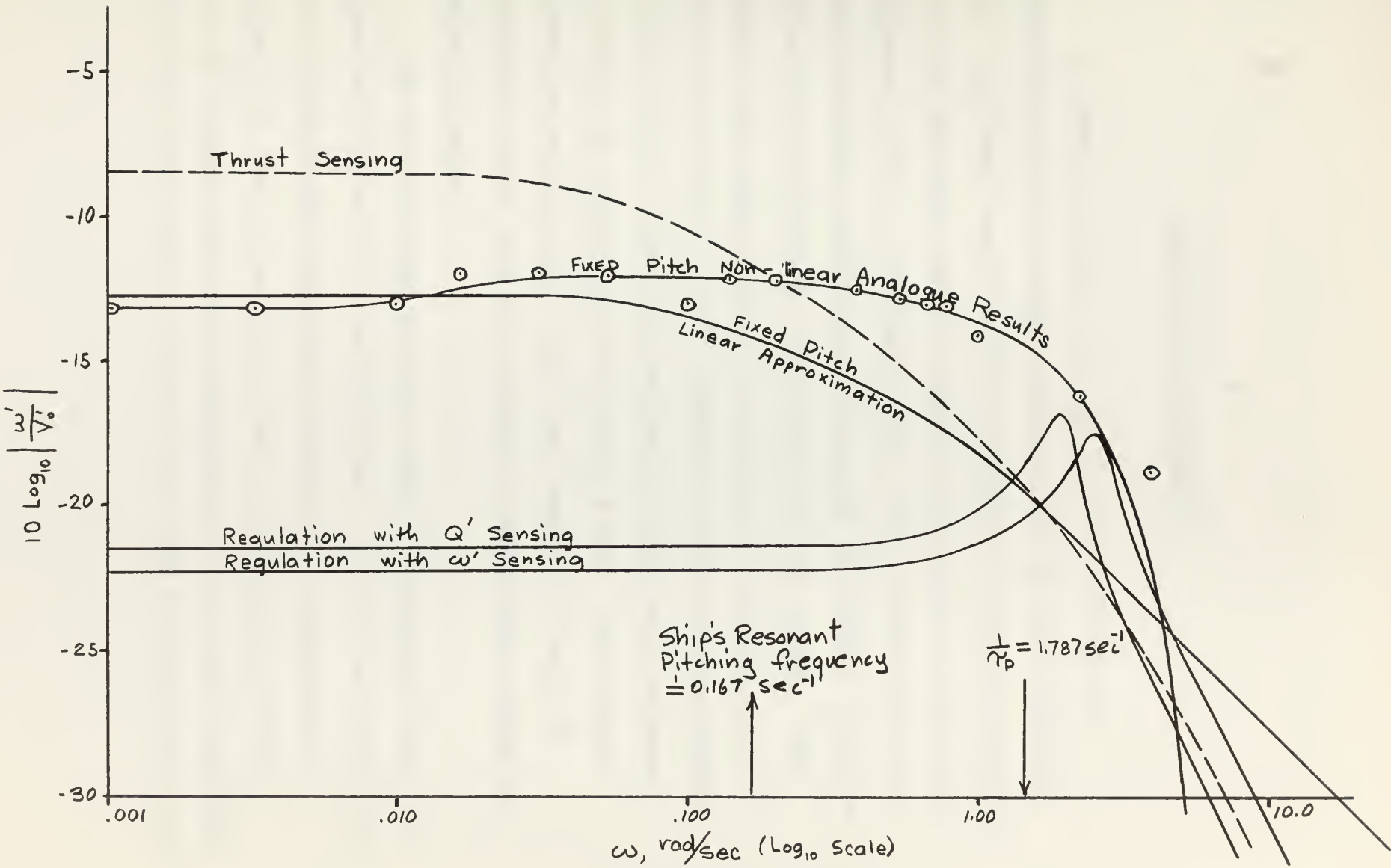

FIGURE E-6

Decilog Plot of Gain for Various Methods of Regulation

V.

DISCUSSION OF RESULTS

As shown in Figure E-6, the fixed pitch response determined on the analogue computer was in good agreement with the linear analysis for frequencies below 0.10 rad/sec. It is of interest that the input levels used to obtain this response curve are extremely high. The minimum value for the fluctuating component of the speed of advance is three volts which corresponds to thirty feet per second. The steady state value of speed of advance is only 16.7 ft/sec. The maximum value of input reached 40 volts corresponding to 400 ft/sec. These high values of input were necessary to obtain an output above the noise level. The results therefore indicate that the linear analysis should be reasonably valid even for moderate fluctuations around the operating point.

Had it been known that the terms containing $\ddot{p}$ and $\dot{V}$ in equation (65) would be insignificant, an analogue eliminating these paths would have been developed. As explained in Appendix D, hum in the $\ddot{p}$ path made the obtaining of data for the closed loop system impossible. The simpler analogue would not have this low signal level path and might have been

more successful. Unfortunately time was not available to reprogram.

The simplifications leading to equation (65) as shown in Appendix C, call for ignoring the term

$$\frac{d}{dt}\left(f_R + \frac{f_r T_\perp \ell\, N}{bR}\right) .$$

This friction term represents an oil flow and since it is discontinuous at $\dot{p} = o$, corresponds to an impulse or hydralic shock. This hydralic shock would very likely be damaging to relief valves and other parts of the system. The introduction of an accumulator to cushion this shock would introduce additional compliance into the system, but as shown in Appendices C and D compliance is relatively unimportant. There are no compliance terms remaining in the final linear analysis.

The simplifications of expression (46) given in Appendix C show that inertia loading is relatively unimportant. Design I has a larger inertia loading because of the relatively larger mass of the control rod compared to the smaller power piston of Design II. The area of the high pressure port delivering full flow to the power piston of Design II would have to be 9.1 square inches to match the output of the variable displacement pump at the same pressure. Since inertia loading is relatively unimportant and since providing a large oil port area would be a difficult engineer-

ing problem, there is little advantage to Design II for this application.

The transfer functions used in comparing the various systems are stable for all frequencies. These transfer functions are based on numerous assumptions that neglect many of the lags and storage elements actually present. They also do not consider nonlinearities such as sliding friction, stiction, saturation, and the nonlinearities present in the propeller characteristics themselves. There is therefore a possibility that the actual hardware might exhibit natural frequencies corresponding to resonances in the remainder of the propulsion system. The lowest frequency of torsional vibration resonance for the Victory Ship (AP2), as measured and reported in Reference 16, is 28 cycles per second or 175 radians per second.

With the restrictions of a maximum pressure of 1000 psi. hydralic pressure, a maximum pump power of 300 HP, and the approximate dimensions of present day controllable pitch propellers, the improvement in shaft RPM regulation over a fixed pitch propeller installation using automatic pitch control corresponds to a reduction in RPM fluctuations by a factor of nine. The improvement in propeller and power plant efficiency would not be great enough for this small an increase in RPM regulation to warrant the installation of such a large and complex system.

Several improvements in the system analyzed might reduce the size of the equipment necessary or improve the system response. The raising of the hydralic pressure would reduce the size of the piston necessary and thereby reduce the capacity of flow necessary from the pump. This would improve the system by reducing the important pump-piston time lag. Increasing the horsepower of the pump also improves the system by decreasing the pump-piston time lag. Compensation in the form of lead or lag networks in the feedback loop would delay the peaking present in the proposed systems and allow a higher closed loop gain and hence a higher degree of regulation.

It is unlikely that the above mentioned changes would result in improvements in system performance to any large degree. If spindle torque could be greatly reduced, the size of the power piston could be reduced and the entire system could be designed with better response and be made smaller. As shown by equation (38), spindle torque consists of many components, each of them large. By increasing hub size the spindle bearing could be made larger and the lever arm of the hub mechanism increased. The application of non-friction bearings might reduce this factor although roller and ball bearings are presently considered unacceptable for naval service due to shock susceptability. If the propeller were designed to operate

at one RPM, the hydrodynamic and centrifugal components might be reduced by careful design. These significant changes might make automatic control of pitch to remove fluctuation in RPM feasible.

As demonstrated by Figure E-6 there is no advantage in sensing either torque or thrust in lieu of RPM when the variable being regulated is RPM. The improvement in regulation offered by RPM sensing is 9.7 decilogs which corresponds to a reduction in fluctuation by a factor of 9.

VI.

CONCLUSIONS

For geared turbine or geared diesel propulsion plants used by the U.S. maritime industry, automatic control of propeller pitch to reduce wave excited RPM fluctuations would be excessively expensive in horsepower, space, and complexity for a small gain in RPM regulation.

Significant reductions in dynamic blade spindle torque through design changes would be necessary to make this scheme practical.

VII.

RECOMMENDATIONS

Automatic pitch control investigation requires a knowledge of spindle torque. Very little is known in this area. It is recommended that future effort be concentrated on the determination of dynamic spindle torque.

A more useful approach to the problem of automatic pitch control would include the presence of engine governing with a view toward developing a system that, with one governor would receive a bridge signal and control pitch and engine throttle setting to achieve the thrust or ship's speed desired by the operator.

VIII.

APPENDIX

APPENDIX A

Derivation of System Equations

1. The Power Plant-Propeller System:

Figure A-1 represents a schematic of the propeller-power plant system.

The equation of motion of this system is

$$Q_E - Q_p - \mathcal{L}_E\omega = (Ji_p' + Ji_E')\dot{\omega} \quad , \qquad (1)$$

where

Q_E = developed engine torque, lb-ft

Q_p = absorbed propeller torque, lb-ft

Ji_p' = effective polar mass moment of inertia of the propeller (includes entrained water), lb-ft-sec^2

Ji_E' = effective polar mass moment of inertia of the engine and gearing referred to the propeller shaft, lb-ft-sec^2

$\mathcal{L}_E$ = mechanical damping in the power plant and gearing, ft-lb-sec.

Q_S = shaft torque, ft-lbs.

ω = shaft rotational speed, radians / second

$\dot{\omega}$ = shaft rotational acceleration, rad/sec^2 .

The torque delivered by the engine is

$$Q_E - \mathcal{L}_E\omega \quad .$$

The shaft torque expression is

$$Q_S = Q_E - \mathcal{L}_E\omega - Ji_E'\dot{\omega} \quad . \qquad (2)$$

Curves of K_Q for most propellers are nearly linear over a wide range of adrance coefficient and pitch ratio. Figure A-2

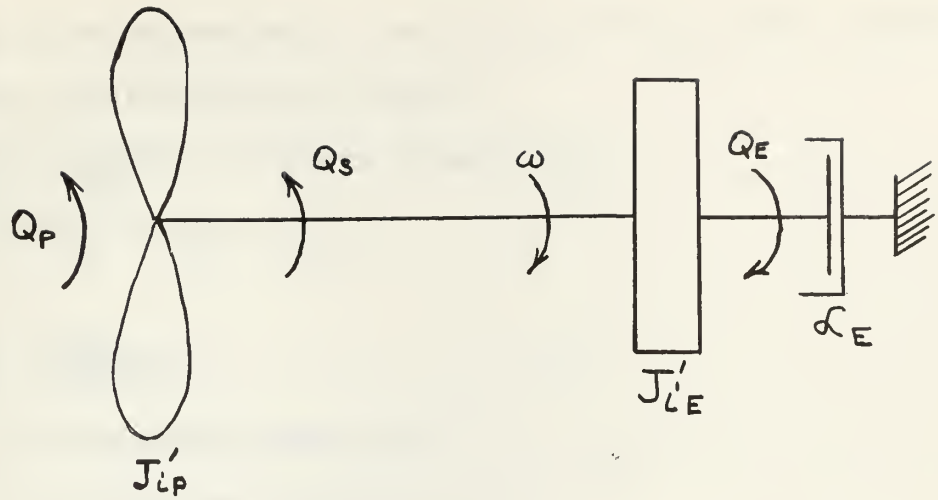

FIGURE A-1

The Propeller-Power Plant System

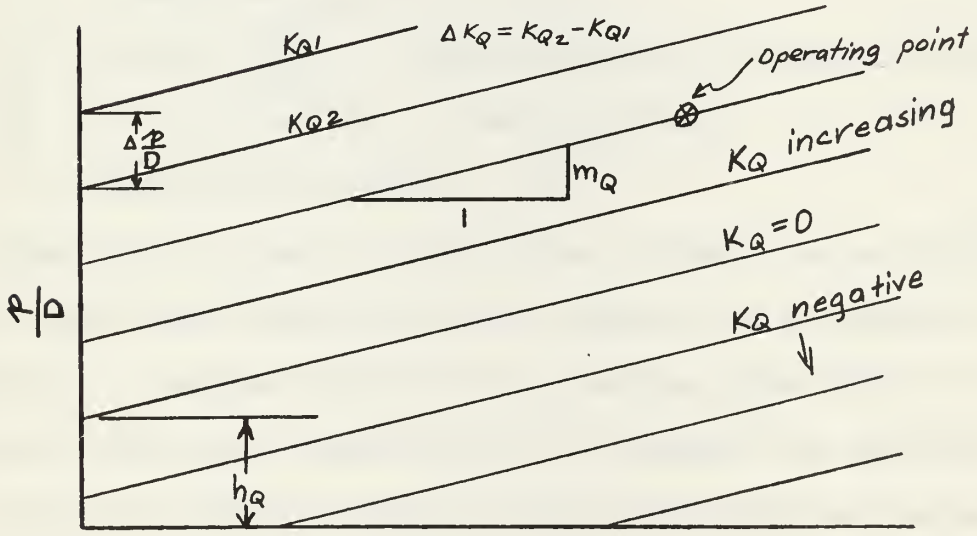

$$J = \frac{V_o}{n D}$$

FIGURE 2

Assumed Linear Torque Coefficient (K_Q) Curves

represents an approximate general set of K_Q curves assuming that they are completely linear.

The equations of these lines are

$$\frac{p}{D} = m_Q J + b_Q K_Q + h_Q \quad , \tag{3}$$

where

$K_Q = \frac{Q\rho}{\rho n^2 D^5}$

p = propeller pitch, ft.

D = propeller diameter, ft.

m_Q = slope of the K_Q curve at the operating point of the true K_Q curve and assumed constant for this analysis, non-dimensional

J = propeller advance coefficient = $\frac{Vo}{nD}$

Vo = speed of advance for the propeller, ft/sec

n = propeller speed, rev./sec

b_Q = ratio $\frac{\Delta \frac{p}{D}}{\Delta K_Q}$, non-dimensional, assumed constant

h_Q = p/D intercept of the K_Q=0 line.

ρ = water mass density 1.024[1]

When m_Q, b_Q, and h_Q correspond to those at an operating point taken from actual propeller curves, the response of the propeller to changes around the operating point will be accurate within the limitations of a steady flow analysis. As the propeller operates farther from this point the assumption of linearity becomes less valid, but is considered sufficiently

---

1. This unit for mass density for water was taken to be consistant with Troost's propeller curves used to determine coefficients of equation (3).

accurate for this study.

Solving equation (3) for Qp,

$$Q_p = \frac{\rho \rho^2 D^4}{b_Q} - \frac{m_Q V_o \rho n D^4}{b_Q} - \frac{h_Q \rho n^2 D^5}{b_Q} \quad . \tag{4}$$

$$\text{Since } n = \frac{\omega}{2\pi} \quad , \tag{5}$$

equation (4) can be written in the form

$$Q_p = K_1 \rho \omega^2 - K_2 V_o \omega - K_3 \omega^2 \quad , \tag{6}$$

where

$$K_1 = \frac{\rho D^4}{4\pi^2 b_Q} \quad , \tag{7}$$

$$K_2 = \frac{m_Q \rho D^4}{2\pi b_Q} \quad , \tag{8}$$

and $$K_3 = \frac{h_Q \rho D^5}{4\pi^2 b_Q} \quad . \tag{9}$$

Substitution of equation (6) into equation (1) completes the derivation of the propeller-power plant system equation.

$$Q_E - K_1 \rho \omega^2 + K_2 V_o \omega + K_3 \omega^2 - \alpha_E \omega = (J i_p' + J i_E') \dot{\omega} \tag{10}$$

The thrust coefficient for most propellers can also be considered linear with respect to ρ/D and J. Again this is accurate for small changes around an operating point and less accurate for large departures from this point. Figure A-3 represents the linear approximation to the actual K_T curves.

The procedure for obtaining thrust as a function of Vo, ω, and p follows in the same manner as used in obtaining the similar expression for Qp.

From the linearized K_T curves

$$\frac{\rho}{D} = m_T J + b_T K_T + h_T \quad . \tag{11}$$

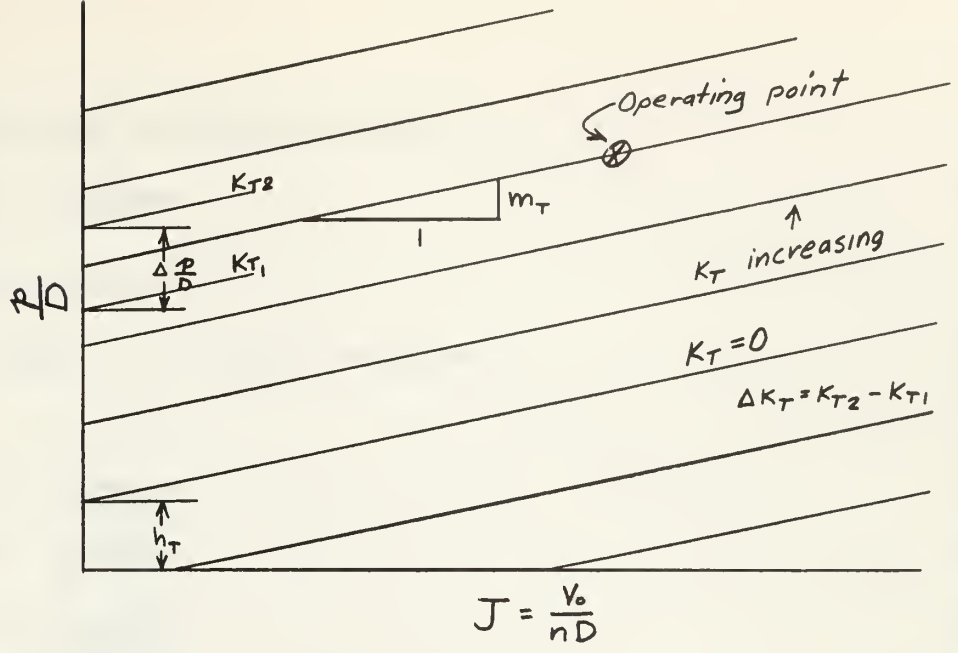

FIGURE A-3

Linear Approximation to K_T Curves

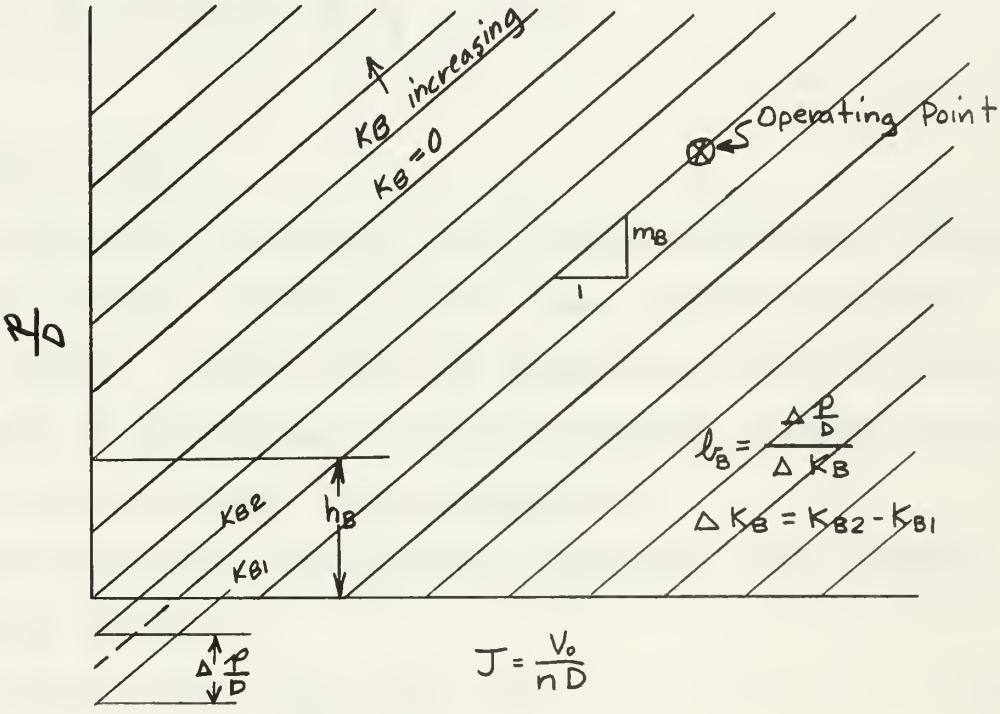

FIGURE A-4

Linearized Hydrodynamic Blade Torque Coefficient Curves

Using the definition of K_T,

$$K_T = \frac{T}{\rho n^2 D^4} \quad , \tag{12}$$

and solving for T.

$$T = K_4 \rho \omega^2 - K_5 V_o \omega - K_6 \omega^2 \tag{13}$$

where

$$K_4 = \frac{\rho D^3}{4\pi^2 h_T} \quad , \tag{14}$$

$$K_5 = \frac{m_T \rho D^3}{2\pi h_T} \quad , \tag{15}$$

and $$K_6 = \frac{h_T \rho D^4}{4\pi^2 h_T} \quad . \tag{16}$$

With $$b = \frac{\Delta \beta_D}{\Delta K_T} \quad , \tag{17}$$

m_T = slope of K_T curve,

and $h_T = \frac{P}{D}$ intercept of $K_Q = 0$ line.

2. Spindle Torque

The equations of motion of any servo system are a function of system loading. Loading in this case consists of blade spindle torque. Torque about the spindle axis can be viewed as composed of hydrodynamic, sliding friction, viscous friction, inertia, and centrifugal force components.

These components are derived separately. The equation for spindle torque is

$$Q_B = Q_{BH} + Q_{BS} + Q_{BV} + Q_{BJ} + Q_{BC} \tag{18}$$

where

Q_B = total spindle torque that must be overcome by the pitch changing mechanism, lb-ft

Q_{BH} = hydrodynamic spindle torque, lb-ft

Q_{BS} = sliding friction torque, lb-ft

Q_{BV} = viscous friction torque, lb-ft

$Q_{BJ} = Ji'_B \omega_B$, lb-ft

Q_{BC} = centrifugal force torque from the mass of the propeller metal, lb-ft.

Very few curves of spindle torque are available. Hydrodynamic spindle torque is a strong function of the spindle axis position relative to the center of hydrodymic pressure. Tests made at M.I.T. show that curves of K_B, where K_B is defined as

$$K_B = \frac{Q_{BH}}{\rho n^2 D^5} \quad , \tag{19}$$

are very nearly linear functions of advance coefficient and pitch ratio just as is K_Q.(2) As with Q_p linear curves for K_B are assumed as shown in Figure A-4, and the expression for Q_{BH} is derived based on this assumption.

For these curves a spindle torque that tends to increase pitch is considered a positive torque.

Proceeding as before,

$$\frac{P}{D} = m_B J + b_B K_{BH} + h_B \tag{20}$$

and

$$Q_{BH} = K_7 \rho \omega^2 - K_8 Vo - K_9 \omega^2 \tag{21}$$

where

$$K_7 = \frac{\rho D^4}{4 \pi^2 b_B} \quad , \tag{22}$$

(2.) Conversation with S. Curtis Powell, March 2, 1962, M.I.T.

$$K_8 = \frac{m_B \rho D^4}{2 \pi b_B} \quad , \tag{23}$$

and $$K_9 = \frac{h_B \rho D^5}{4 \pi^2 b_B} \quad . \tag{24}$$

The spindle is not a journal loaded in the normal manner. Propeller thrust acts at a considerable moment arm tending to rotate the spinde about an axis perpendicular to its centerline as shown in Figure A-5.

If the bearing were normally loaded the friction torque would be

$$fPr \quad , \quad \text{lb-ft} \quad ,$$

where

f = coefficient of journal friction

P = bearing load, lb

r = spindle radius, ft.

$T_\perp$ = total thrust on blade perpendicular to the spindle axis, lb.

An approximate expression for spindle sliding friction is

$$Q_{BS} = fr \frac{T_\perp \ell}{b} N \tag{25}$$

where

ℓ = lever arm from center of thrust on the blade to the center of the spindle bearing, ft.

b = spindle bearing length, ft.

N = number of blades

Sliding and static friction are assumed to be the same.

Blade viscous torque can be expressed as

$$Q_{BV} = \mathcal{L}_B \omega_B N \tag{26}$$

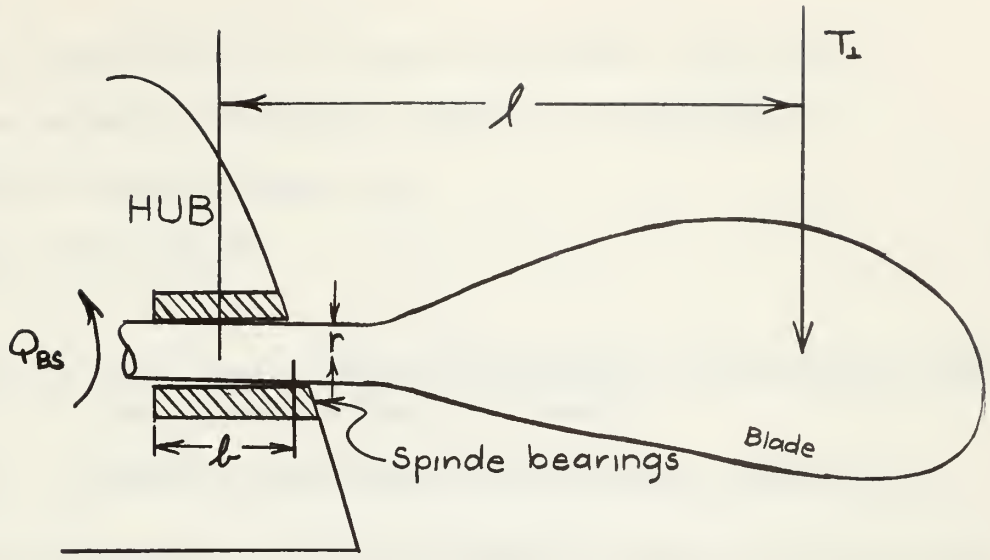

FIGURE A-5

Schematic Indicating Blade Sliding Friction (Q_{BS})

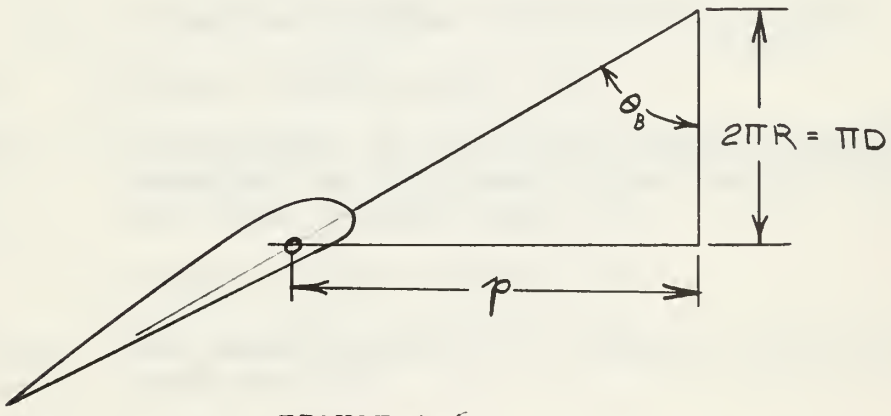

FIGURE A-6

The Relationship Between Pitch and Blade Angle

where

α_B = coefficient of viscous friction, lb-ft-sec.

ω_B = spindle rotational velocity, radians/sec.

Blade inertia torque is

$$Q_{BJ} = Ji'_B \dot{\omega}_B N \quad , \tag{27}$$

where

Ji'_B = polar mass moment of inertia of the blade about the spindle axis, lb-ft-sec^2

$\dot{\omega}_B$ = spindle rotational acceleration, rad/sec^2 .

The expression for blade spindle torque as derived by Boswell and others is [3]

$$Q_{BC} = -\rho_P \omega^2 N \left[\int_{hub}^{tip} A x y \, dr + \int_{root}^{tip} \frac{(I_{max} - I_{min}) \sin 2\alpha \, dr}{2} \right] \tag{28}$$

where

ρ_P = mass density of the blade material, lb-sec^2/ft^4

ω = propeller angular velocity in rad/sec.

A = blade section area, ft^2

x,y = coordinates of the blade section centroid measured in the plane of the section from the blade spindle axis, ft.

r = radius of the section, ft.

I_{MIN} = the minimum moment of inertia of the blade section, ft^4

---

3. Robert J. Boswell, A Method of Calculating the Spindle Torque of a Controllable-Pitch Propeller at Design Conditions. David Taylor Model Basin Report No. 1529, Aug. 1961, pp. 31-34.

I_{MAX} = the maximum moment of inertia of the blade section, ft^4

α = pitch angle of the section from its major axis, and is a function of both r and p.

Q_{BC} = centrifugal component of blade torque, positive tending to rotate pitch ahead., lb-ft

Equation (28) is not readily adapted to analogue computation. Several simplifying assumptions are necessary to make it so.

Let θ_B be the pitch angle in radians at the seven tenths radius. This angle corresponds to the "pitch" of the blade as shown in Figure A-6.

α in equation (21) will be greater than θ_B near the root and less than θ_B at the tip.

Assume $\alpha = \theta_B$. This assumes a constant pitch angle over the blade length. Equation (28) can then be written:

$$-Q_{BC} = \rho_p \omega^2 N \int_{hub}^{tip} A\,xy\,dr + \rho_p \omega^2 \sin 2\theta_B \int_{root}^{tip} \frac{(I_{MAX}-I_{MIN})}{2}\,dr \qquad (29)$$

From Figure A-6 is can be seen that

$$\frac{p}{\pi D} = \tan \theta_B \qquad (30)$$

and $$\therefore \quad \theta_B = \tan^{-1} \frac{p}{\pi D} \quad , \qquad (31)$$

whose expansion is

$$\theta_B = \frac{p}{\pi D} - \frac{1}{3}\left(\frac{p}{\pi D}\right)^3 + \cdots \quad , \qquad (32)$$

$$\text{for } \frac{p}{\pi D} < 1 \quad .$$

The expansion for Sin $2\theta_B$ is

$$\text{Sin } 2\theta_B = 2\theta_B - \frac{(2\theta_B)^3}{3!} + \cdots \tag{33}$$

Equating the first terms of these expansions,

$$\frac{2\rho}{\pi D} \doteq \text{Sin } 2\theta_B \tag{34}$$

This assumption will introduce an error for this component of spindle torque that is sometimes conservative and sometimes not conservative since the total spindle torque is a sum of components with changing signs leading to a sum that also changes sign. The maximum error will occur for large values of $\frac{\rho}{D}$. For the case studies, $\left(\frac{\rho}{D}\right)_{MAX} = 1.1$

For this case

$$\frac{2\rho}{\pi D} = 0.705,$$

and $\text{Sin } 2\theta_B = 0.644$.

With these assumptions equation (29) reduces to

$$Q_{BC} = -K_{10}\omega^2 - K_{11}\omega^2 \tag{35}$$

where

$$K_{10} = N \rho_P \int_{hub}^{tip} Axy \, dr \tag{36}$$

and

$$K_{11} = N\pi D\rho_P \int_{hub}^{tip} (I_{MAX} - I_{MIN}) \, dr \tag{37}$$

Substituting equations (21), (25), (26), (27), and (36) into equation (18) ,

$$Q_B = K_7 \rho \omega^2 - K_8 V_o \omega - K_9 \omega^2 \pm f \frac{r T_1 l N}{b} + \alpha_B \omega_B N +$$

$$J i'_B \dot{\omega}_B - K_{10} \omega^2 - K_{11} \omega^2 \rho \quad . \qquad (38)$$

Where N = number of blades

The double sign before the fourth term, $(\frac{f r T_1 l}{b})$, is to indicate that this term changes its sign such that friction torque resists spindle motion. This term will take on the same sign as the viscous friction term, $\alpha_B \omega_B$.

3. The Pitch Setting Mechanism

Two designs for the pitch setting mechanism are investigated. Both are hydralic. Design I is a pump controlled system using a variable displacement pump and a control rod running through the propeller shaft and is shown schematically in Figure A-7. Design II is a valve controlled system with the power piston within the hub. Design II includes a safety spring to make the propeller fail safe in case of loss of hydralic pressure and is shown in Figure A-8.

The relationship between pitch and control rod or piston position depends on the particular hub mechanism involved. Several designs are in use. Figures A-8 and A-7 show two possible methods. Figure A-7 shows two additional methods also in use.

For a given hub diameter the parameter R in each mechanism will be approximately the same. The ratio $\frac{X_c}{R}$ for a given pitch

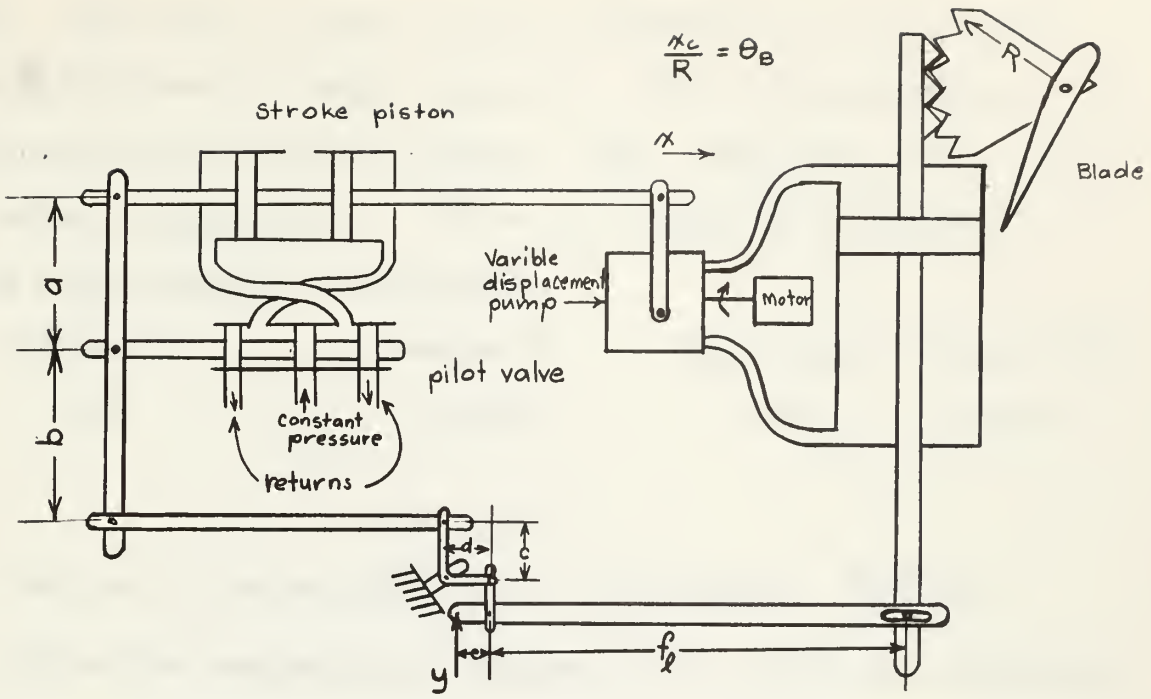

FIGURE A-7

Design I Schematic

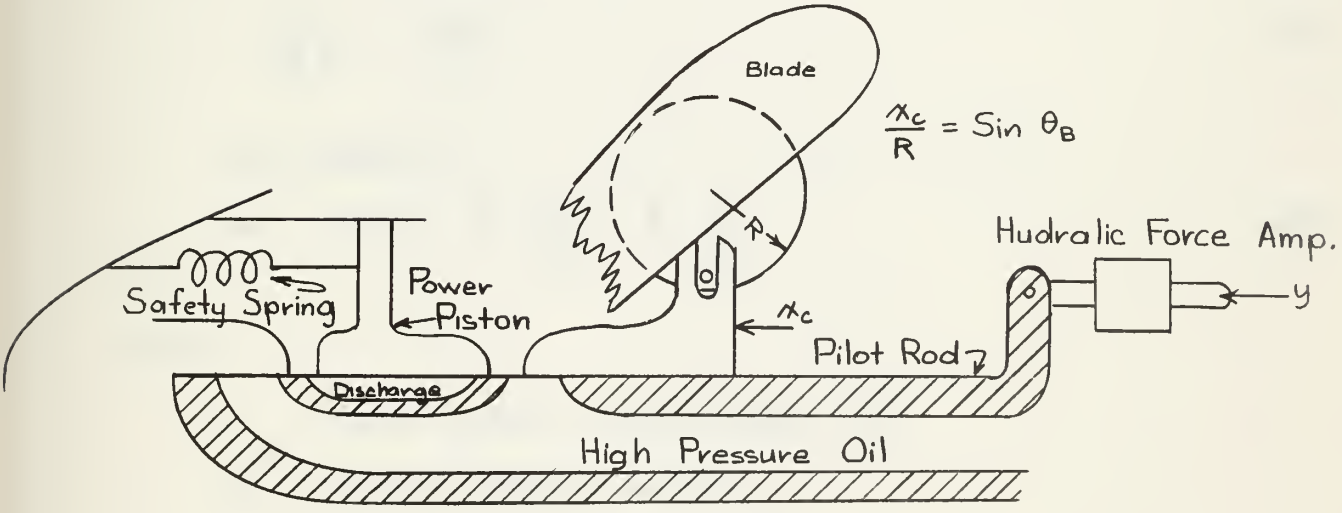

FIGURE A-8

Design II Schematic

ratio ρ/D will be only slightly different for any of the four mechanisms for small values of ρ/D. The greatest difference will occur for large ρ/D. Table A-1 shows the value of $\chi c/R$ for a $\rho/D = 1.5$, which is as large a pitch ratio usually encountered.

Design I	Design II	Fig. 9-A(a)	Fig 9-A(b)
.478	.430	.466	.431

Table A-1

Values of the ratio $\frac{\chi c}{R}$ for a pitch ratio $\rho/D = 1.5$

Since the mechanism of Figure 9-A(a) yields the simplest relationship between pitch and control rod displacement, it is used throughout the study. The overall results, however, will apply with reasonable accuracy to any of the hub mechanisms shown.

$$\therefore \frac{\rho}{\pi D} = \frac{\chi c}{R} \tag{39}$$

For Design I,

$$Kpx = \dot{x}_c A_R + F_c \frac{K_L}{A_R} + \dot{F}_c \frac{K_c}{A_R} \tag{40}$$

where

x = pump control displacement, in.

Kp = pump constant, in^3/in

Kpx = flow from the pump, in^3

x_c = control rod displacement, in

$\dot{x}_c$ = velocity of control rod, in/sec

A_R = control rod piston area, in^2

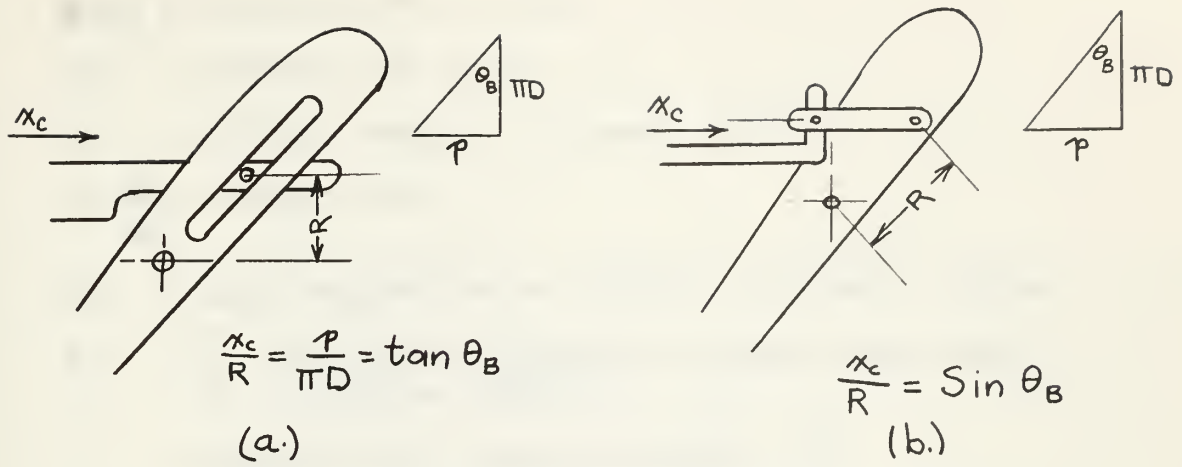

FIGURE A-9

Two Additional Hub Mechanisms

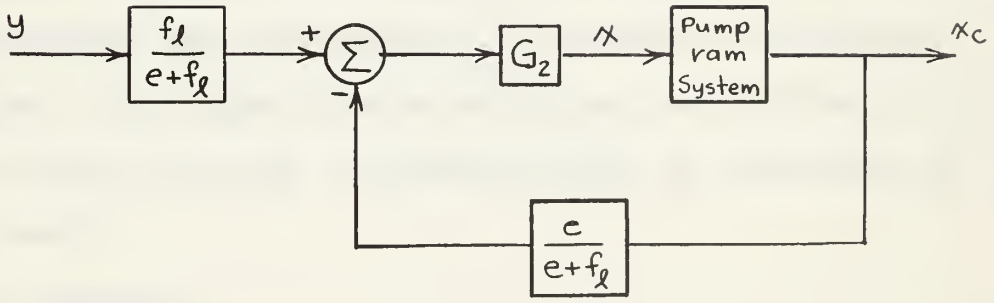

FIGURE A-10

Design I Block Diagram

$\dot{x}_c A_R$ = piston flow, in^3/sec

F_c = control rod force, lb.

K_L = leakage constant of pump, $in^5/16$

$F_c \frac{K_L}{A_R}$ = leakage flow

$\dot{F}_c$ = time derivative of control rod force, lb/sec

$K_c = \frac{V}{B}$ = compliance constant of the system under pressure, in^5/lb

V = volume of oil under pressure, in^3

$B = \frac{\Delta V/V}{P}$ = bulk modulus of hydralic fluid, $\frac{in}{lb}$

P = hydralic pressure, lb/in^2

$\dot{F} \frac{K_c}{A_R}$ = compliance flow, in^3/sec .

Equation (40) neglects leakage around the control rod piston and expansion of the hydralic piping. These factors can easily be accounted for increasing K_L to account for piston leakage, and increasing K_c to account for piping expansion. The compression of entrained air bubbles in the hydralic fluid can also be accounted for by increasing K_c appropriately.

For Design I,

$$F_{c_Q} = \frac{1}{R} Q_B \quad , \tag{41}$$

where F_{c_Q} is that component of control rod force transmitted from spindle torque, lb.

Using equations (39), (40), and (41) the expression

for the dynamic motion of the pump-propeller system is

$$K_P x = \underbrace{\dot{p}\frac{12R}{\pi D}A_R}_{\text{Input}} + \underbrace{\frac{K_L}{A_R}\left[\frac{K_7 p\omega^2}{R} - \frac{K_8 V_o \omega}{R} - \frac{K_9\omega^2}{R} \pm \left(f_R + \frac{f_r T_L l N}{\eta R}\right) + \frac{\dot{p}}{\pi D}\left(\frac{\alpha_B N}{R} + \mathcal{N}_R R\right) + \frac{\ddot{p}}{\pi D}\left(\frac{J_{LB}' N}{R} + M_C R\right) - \frac{K_{10}\omega^2}{R} - \frac{K_{11}\omega^2 p}{R}\right]}_{\text{Ram Flow}} + \underbrace{\frac{K_c}{A_R}\left\{\frac{d}{dt}\left[\left(\frac{K_7 p\omega^2}{R} - \frac{K_8 V_o \omega}{R} - \frac{K_9\omega^2}{R} \pm \left(f_R + \frac{f_r T_L l N}{\eta R}\right) - \frac{K_{10}\omega^2}{R} - \frac{K_{11}\omega^2 p}{R}\right)\right] + \frac{\ddot{p}}{\pi D}\left(\frac{\alpha_B N}{R} + \mathcal{N}_R R\right) + \frac{\dddot{p}}{\pi D}\left(\frac{J_{LB}' N}{R} + M_C R\right)\right\}}_{\text{Leakage Flow}} \quad (42)$$

compliance flow

where R = crank radius, ft.

f_R = control rod ram sliding friction, lb

$\mathcal{N}_R$ = control rod and piston, viscous friction coefficient, $\frac{\text{lb-sec}}{\text{ft}}$

M_C = control rod effective mass, $\frac{\text{lb-sec}^2}{\text{ft}}$

For Design II, as shown in Figure A-8 the equation for flow to the power piston is:

$$(y-x_c)\, L\, K_X - \dot{x}_c A_R + F_c\frac{K_L}{A_R} + \dot{F}_c\frac{K_c}{A_R} \quad . \qquad (43)$$

Where

y = pilot piston displacement, in

L = inlet port width

K_X = valve constant, in^3/in

The control rod force in this case is the same as with Design I (the values of parameters will vary) with the exception

of an additional term contributed by the safety spring.

The resulting equation for Design II is:

$$
\begin{aligned}
\text{Input} \qquad & \text{Ram Flow} \qquad \text{Mechanical Feedback} \qquad \text{Leakage Flow} \\
y L K_x = {} & \dot{x}_c A_R + x_c L K_x + \frac{K_L}{A_R}\left[\frac{(k_7-K_{11})}{R}\rho\omega^2\right. \\
& - \frac{K_B V_o \omega}{R} - \frac{(k_9+K_{10})}{R}\omega^2 \pm \left(f_R + \frac{f_r T_\perp \ell N}{b R}\right) \\
& + \frac{\dot{\rho}}{\pi D}\left(\frac{\sigma_B N}{R} + \mu_R R\right) + \frac{\ddot{\rho}}{\pi D}\left(\frac{J'_{LB} N}{R} + M_c R\right) \\
& \left. \underset{\text{Spring term}}{+ k R (c-\rho)}\right] + \underset{\text{Compliance flow}}{\frac{k_c}{A_R}}\left\{\frac{d}{dt}\left[\frac{(k_7-K_{11})}{R}\rho\omega^2\right.\right. \\
& - \frac{K_B V_o \omega}{R} - \frac{(k_9+K_{10})\omega^2}{R} \pm \left(f_R + \frac{f_r T_\perp \ell N}{b R}\right)\Bigg] \\
& + \frac{\ddot{\rho}}{\pi D}\left(\frac{\sigma_B N}{R} + \mu_R R\right) - \dot{\rho}\,\underset{\text{Spring term}}{\frac{k R}{\pi D}}\Bigg\}
\end{aligned}
\tag{44}
$$

Where

k = spring constant, lb/in

$c\frac{kR}{\pi D}$ = spring force when $\rho = 0$, lb

The pilot valve-stroke piston system shown in Figure A-7 for Design I is standard and is fully analyzed in Reference 33. It can easily be shown that the time constant of such a system, loaded with 0.4 lb-sec^2 mass and supplied with 1000 lb/in^2 pressure oil will have time constants less than 0.1 sec even with excessive volumes of oil under

pressure. Since the transients of this portion of the system decay in a small fraction of the remainder of the system transients, the pilot-valve-stroke piston system can be viewed as a simple gain.

The feedback provided by the mechanical linkages of Design I are shown in Figure A-10.

From Figure A-10 it is evident that

$$x = G_2 \left(y \frac{f_l}{e+f_l} - \frac{x_c e}{e + f_l} \right) \quad . \tag{45}$$

Substituting equation (45) into (42); using relation (39),

Input — Ram Flow — Mechanical Feedback

$$\frac{K_p G_2 f_l y}{e+f_l} = \dot{p} \frac{12 R A_R}{\pi D} + \frac{12 R e K_p G_2}{(e+f_l)\pi D} p$$

Leakage flow

$$+ \frac{K_L}{A_R} \left[\frac{(K_7 - K_{11})}{R} p\omega^2 - \frac{K_8 V_0 \omega}{R} - \frac{(K_9 + K_{10})}{R} \omega^2 \right.$$

$$\pm \left(f_R + \frac{f_r T_1 l N}{h R} \right) + \frac{\dot{p}}{\pi D} \left(\frac{\alpha_B N}{R} + \mu_R R \right)$$

$$\left. + \frac{\ddot{p}}{\pi D} \left(\frac{J_i \beta N}{R} + M_c R \right) \right] + \frac{K_c}{A_R} \left\{ \frac{d}{dt} \left[\frac{(K_7 - K_{11})}{R} p\omega^2 \right.\right.$$

Compliance flow

$$- \frac{K_8 V_0 \omega}{R} - \frac{(K_9 + K_{10})}{R} \omega^2 \pm \left(f_R + \frac{f_r T_1 l N}{h R} \right) \Bigg]$$

$$\left. + \frac{\ddot{p}}{\pi D} \left(\frac{\alpha_B N}{R} + \mu_R R \right) \right\} \tag{46}$$

With the exception of the extra terms envolving the spring force in equation (44) equations (46) and (44) are of exactly the same form. They are arranged so that the analogue can be easily drawn. The analogue diagram for Design I is obtained from the analogue diagram of Design II by simply removing the two spring force feedback loops and adjusting parameters to match the actual system.

APPENDIX B

Determination of System Parameters

1. Ship Characteristics

The Victory Ship (AP2) was chosen as a prototype to obtain representative parameters for the system. The Troost B4-55 propeller curves were used to determine the propeller operating point for the Victory Ship specifications. Values for wake fraction were taken from references 16 and 17.

These values are summarized as follows:

Ship, victory, AP2

SHP .....6000 hp.

D, propeller diameter .....18.25 ft.

Speed, V .....15.5 knots

RPM, n x 60 .....100 rpm

Number of propeller blades, N.....4

Effective horsepower, EHP .....4650 hp.

Thrust, T_o .....98,000 lb.

Propeller Torque, Q_p.....3.1×10^5 lb-ft

Thrust wake fraction, ω_T 0.348

Torque wake fraction, ω_Q 0.368

Thrust coefficient, K_T 0.310

Torque coefficient, K_Q 0.054

Pitch ratio, P/D 1.15

Mean width ratio, MWR 0.259

Speed of advance, Vo .....16.7 ft/sec

2. Propeller Characteristics

The Troost curves for K_Q were then linearized about the operating point. The resulting linear approximation to these curves are shown in Figure B-1 and B-2.

Values for K_1, K_2, K_3, K_4, K_5, and K_6 were then obtained by substitution of the appropriate values into equations (7), (8), (9), (14), (15), and (16) respectively.

$$K_1 = \frac{\rho D^4}{4\pi^2 b_Q} = \frac{(1.024)(18.24)^4}{40\pi^2} \text{ lb-sec}^2 = 288 \text{ lb-sec}^2 \quad (7)$$

$$K_2 = \frac{m_Q \rho D^4}{2\pi b_Q} = \frac{(.476)(1.024)(18.24)^4}{20\pi} \text{ lb-sec}^2$$

$$= 863 \text{ lb-sec}^2 \quad (8)$$

$$K_3 = \frac{h_Q \rho D^5}{4\pi^2 b_Q} = \frac{.35(1.024)(18.25)^5}{40\pi^2} \text{ lb-sec}^2\text{-ft}$$

$$= 1840 \text{ lb-sec}^2\text{=ft} \quad (9)$$

$$K_4 = \frac{\rho D^3}{4\pi^2 b} = \frac{(1.024)(18.25)^3}{\pi^2 (.2)} \frac{\text{lb-sec}^2}{\text{ft}}$$

$$= 69.5 \text{ lb-sec}^2\text{-ft} \quad (14)$$

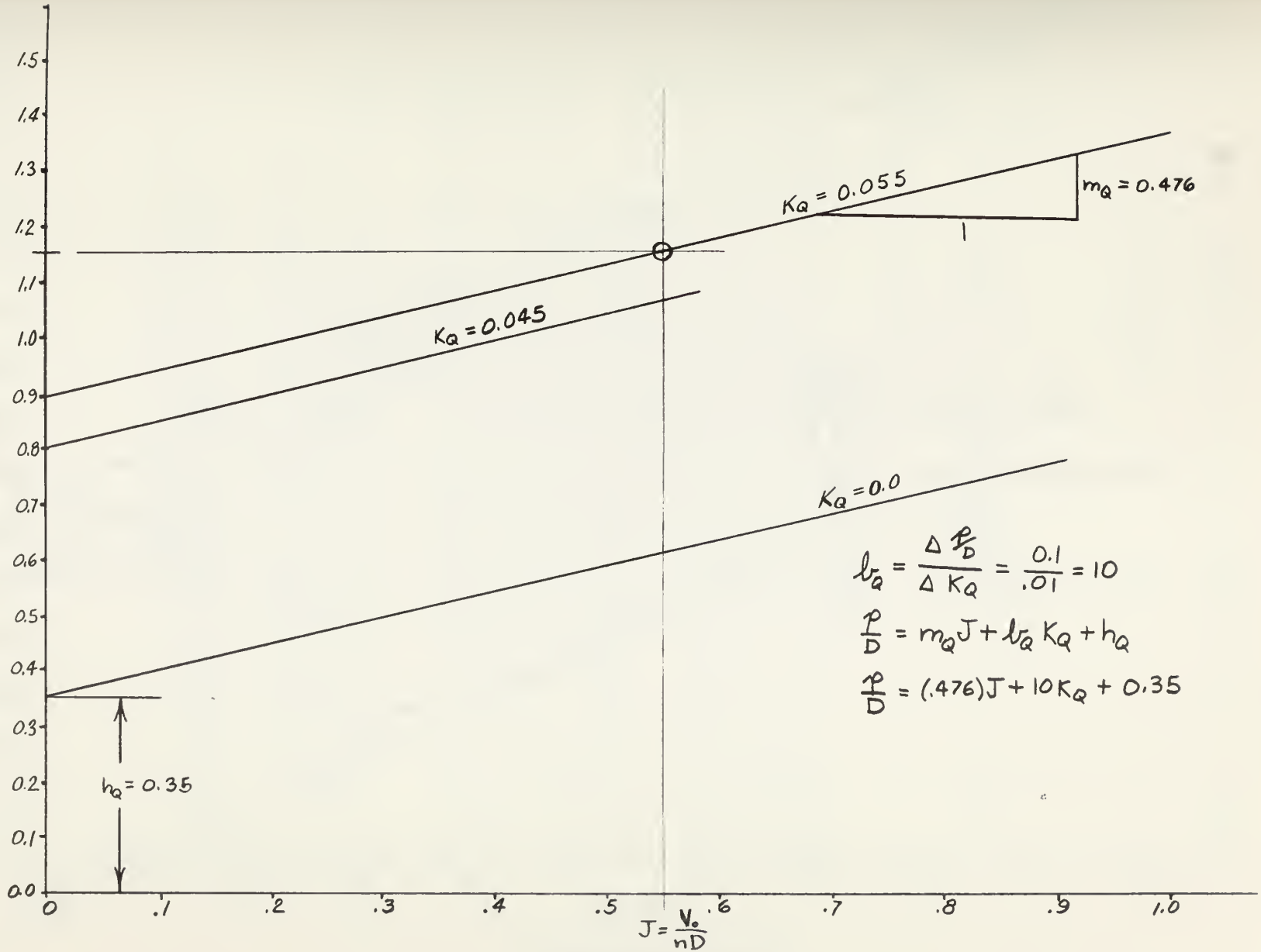

FIGURE B-1
Linearized K_Q Curves

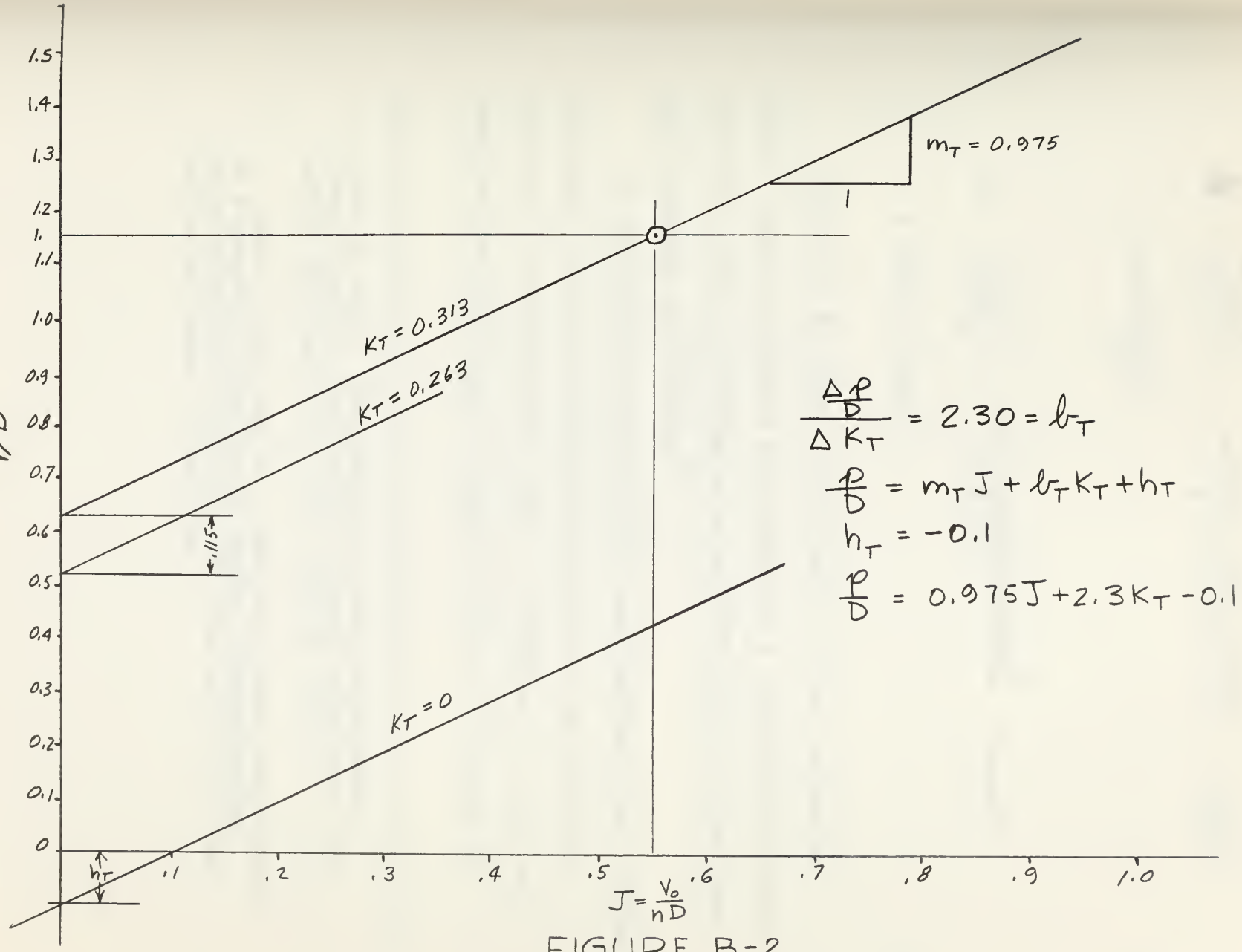

$$\frac{\frac{\Delta P}{D}}{\Delta K_T} = 2.30 = b_T$$

$$\frac{P}{D} = m_T J + b_T K_T + h_T$$

$$h_T = -0.1$$

$$\frac{P}{D} = 0.975 J + 2.3 K_T - 0.1$$

FIGURE B-2

Linearized K_T Curves

$$K_5 = \frac{m_T \rho D^3}{2\pi b_T} = \frac{(.975)(1.024)(18.25)^3}{2\pi\,(2.5)} \quad \frac{\text{lb-sec}^2}{\text{ft}}$$

$$= 420 \frac{\text{lb-sec}^2}{\text{ft}} \tag{15}$$

$$K_6 = \frac{h_T \rho D^4}{4\pi^2 b_T} = \frac{(0.1)(1.024)(18.25)^4}{9.2\,\pi^2} \quad \text{lb-sec}^2$$

$$= 125.2 \text{ lb-sec}^2 \tag{16}$$

Curves of K_8 were not available for any propeller. Rupp's data for control rod forces on a controllable pitch propeller while operating on a tug (YTB-502) in free route were analyzed as follows:[4]

An approximate wake fraction was computed from a formula relating the block coefficient of the tug to the wake fraction.[5] The propeller speed of advance, Vo, was then computed for the range of speeds tested. The speed of

---

4. Lewis A. Rupp, "Controllable Pitch Propellers," Transations of the Society of Naval Architects and Marine Engineers, Vol. 56, 1948. pp. 272.

5. S. Curtis Powell and W.V. Bassett, "Practical Aspects of Torsional Vibration in Marine Geared-Turbine Propulsion Units," Society of Naval Architects and Marine Engineers, March 1944.

advance, J, was then computed from its definition and the available data for each pitch ratio and speed. The corresponding control rod force was taken from curves given in Rupp's paper. Since these forces represent both the hydrodynamic and centrifugal components of torque converted to force, the centrifugal force component of torque was subtracted from the total torque obtained from this force. The blade torque coefficient for each pitch ratio and advance coefficient was then computed from its definition, equation (19). The results were then plotted and found to be very nearly linear as shown in Figure B-3. The tabulation of the calculations leading to the curves of K_8 are shown in Table B-1.

As stated in Appendix A, the blade hydrodynamic spindle torque is a strong function of spindle position. The actual values for K_8 could be shifted up and down the family of K_8 curves by shifting this spindle axis. For the purpose of this study the K_8 family of curves were assumed to be oriented such that the curve for zero torque intersected the origin of the pitch ratio - advance coefficient plot. This can be justified only in that a propeller <u>could</u> be made to give this result. This design would give a much more reasonable torque in the region of normal operation than merely using the tug propeller curves. The tug propeller was designed for a pitch ratio of about 0.7 in lieu of the Victory Ship with a $P/D \doteq 1.15$. The slope

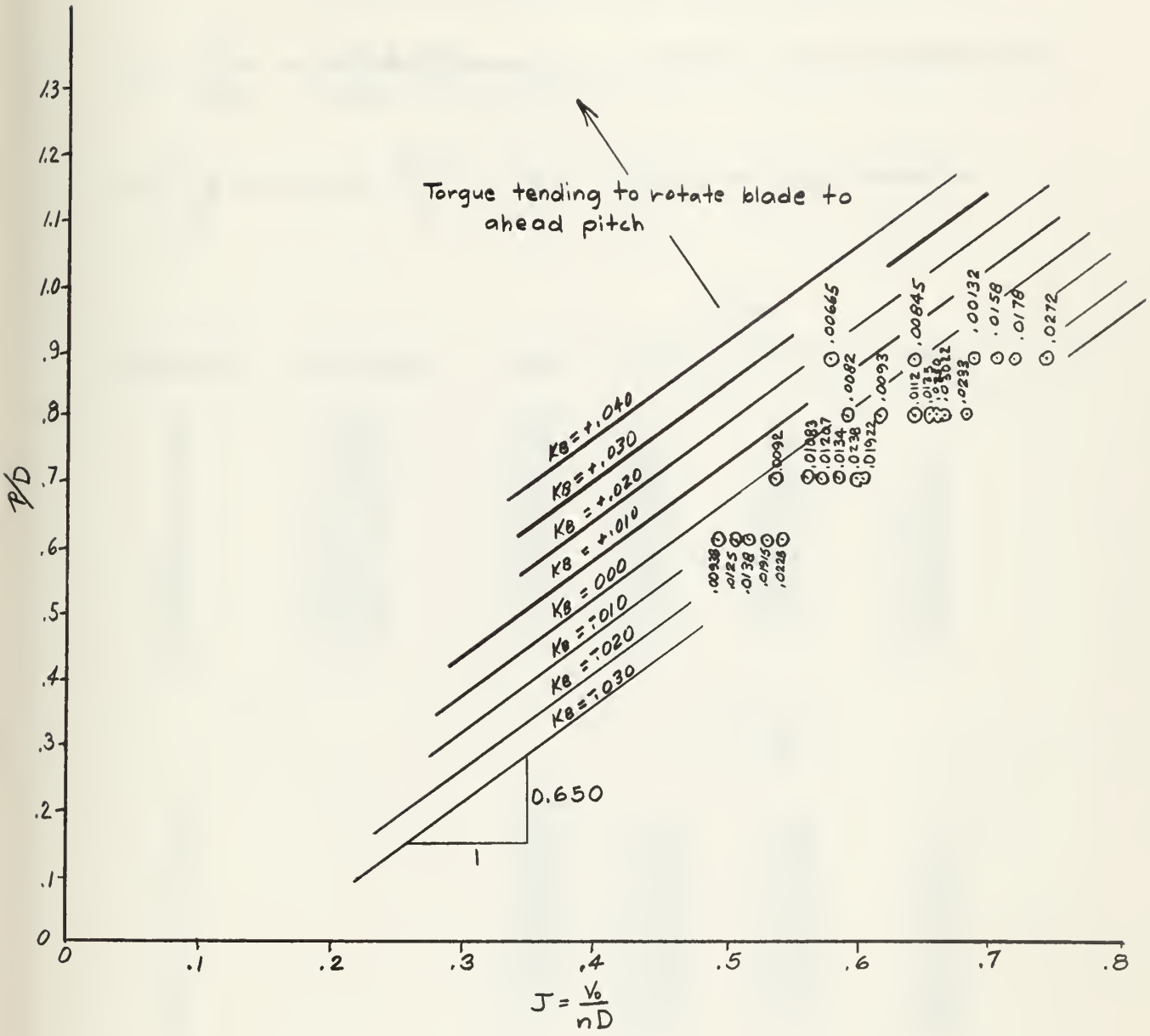

FIGURE B-3

Derived K_B Curves for YTB-502

TABLE B-1

Tabulation of YTB502 Free Route Trial Calculations Leading to K_B Curves

$$C_B = \frac{\forall}{LBD} = \frac{332 \times 35}{(90.64)(25)(9.72)} = 0.527 = \text{Block coefficient}$$

$$w = \frac{C_B}{2} - 0.10 \doteq \frac{.527}{2} - 0.10 \doteq 0.164 = \text{wake fraction}$$

V_S, knots	V_9 ft/sec	RPM p=5.8	p=6.7	p=7.6	p=8.5
5	7.05	82	-	-	-
6	8.46	100	89	80	-
7	9.89	118	103	92	84
8	11.30	136	120	108	99
9	12.70	155	137	123	111
10	14.10	176	155	140	126
11	15.51	200	175	160	143
12	16.92	-	200	182	166
13	18.35	-	-	-	200
		$J = \frac{V_o}{nD}$			
5		.544	-	-	-
6		.535	.600	.668	-
7		.529	.606	.679	.743
8		.524	.595	.661	.721
9		.516	.585	.652	.723
10		.505	.574	.635	.706
11		.491	.560	.614	.687
12		-	.536	.588	.644
13		-	-	-	.581

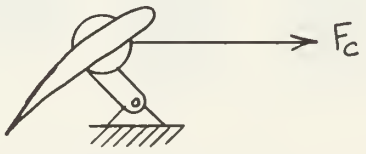

FIGURE B-5

YTB-502 Hub Mechanism

$F_c \times 10^{-3}$ lbs (includes centrifugal force component)

V_S P/D	.610	.705	.800	.895
5	8.8	-	-	-
6	9.5	9.0	9.0	-
7	11.2	9.9	9.4	9.1
8	13.6	11.1	9.9	9.5
9	16.5	12.7	10.6	9.6
10	20.1	14.4	11.6	10.1
11	22.5	16.8	13.1	11.3
12	-	20.8	15.5	13.2
13	-	-	-	17.5

Q_{BH} ft-lb-x10^{-3}, centrifugal force component subtracted

5	4.15	-	-	-
6	4.38	4.20	4.24	-
7	5.06	4.50	4.33	4.22
8	6.05	4.91	4.46	4.28
9	7.28	5.51	4.54	4.16
10	8.75	6.37	4.82	4.20
11	9.20	7.31	5.25	4.47
12	-	9.00	6.00	5.14
13	-	-	-	6.51

$$K_B = \frac{Q_B}{\rho n^2 D^5}$$

Note: ρ =1.024 to match Troost's curves

Y_S P/D	.610	.705	.800	.895
5	.0278	-	-	-
6	.01915	.0238	.0302	-
7	.01604	.01922	.0233	.0272
8	.01481	.01550	.01740	.0198
9	.01379	.01340	.01354	.01538
10	.01291	.01207	.01112	.01200
11	.00938	.01083	.00930	.00994
12	-	.00910	.00820	.00845
13	-	-	-	.00665

(m_B) and spacing (b_B) were assumed to remain the same. The resulting linearized approximation is shown in Figure B-4.

Values for K_7, K_8, and K_9 were then obtained by substitution of the appropriate constants into equations (22), (23), and (24) as follows:

$$K_7 = \frac{\rho D^4}{4\pi^2 b_B} = \frac{(1.024)(18.25)^4}{4\pi^2(6)} = 480 \frac{\text{lb-sec}^2}{\text{ft}} \qquad (22)$$

$$K_8 = \frac{m_B \rho D^4}{2\pi b_B} = \frac{(.650)(1.024)(18.25)^4}{2\pi(6)} = 1959 \text{ lb-sec} \qquad (23)$$

$$K_9 = \frac{h_B \rho D^5}{4\pi^2 b_B} = \frac{(0)(1.024)(18.25)^5}{4\pi^2 (6)} = 0 \qquad (24)$$

Sliding friction, as represented by equation (25), contains the thrust perpendicular to the spindle axis. This is the resultant of force vectors in the plane of the propeller disc as well as perpendicular to it. These vectors change with pitch, speed of advance, and RPM. These dependencies are difficult to account for, and $T_\perp$ was assumed equal to T_o and constant. The dimensions assumed for bearing length and diameter are based on dimensions scaled from existing CCP hub mechanisms as shown in Ref. 11. In each case the dimension was assumed to be a value giving the least final value for sliding friction force. A friction

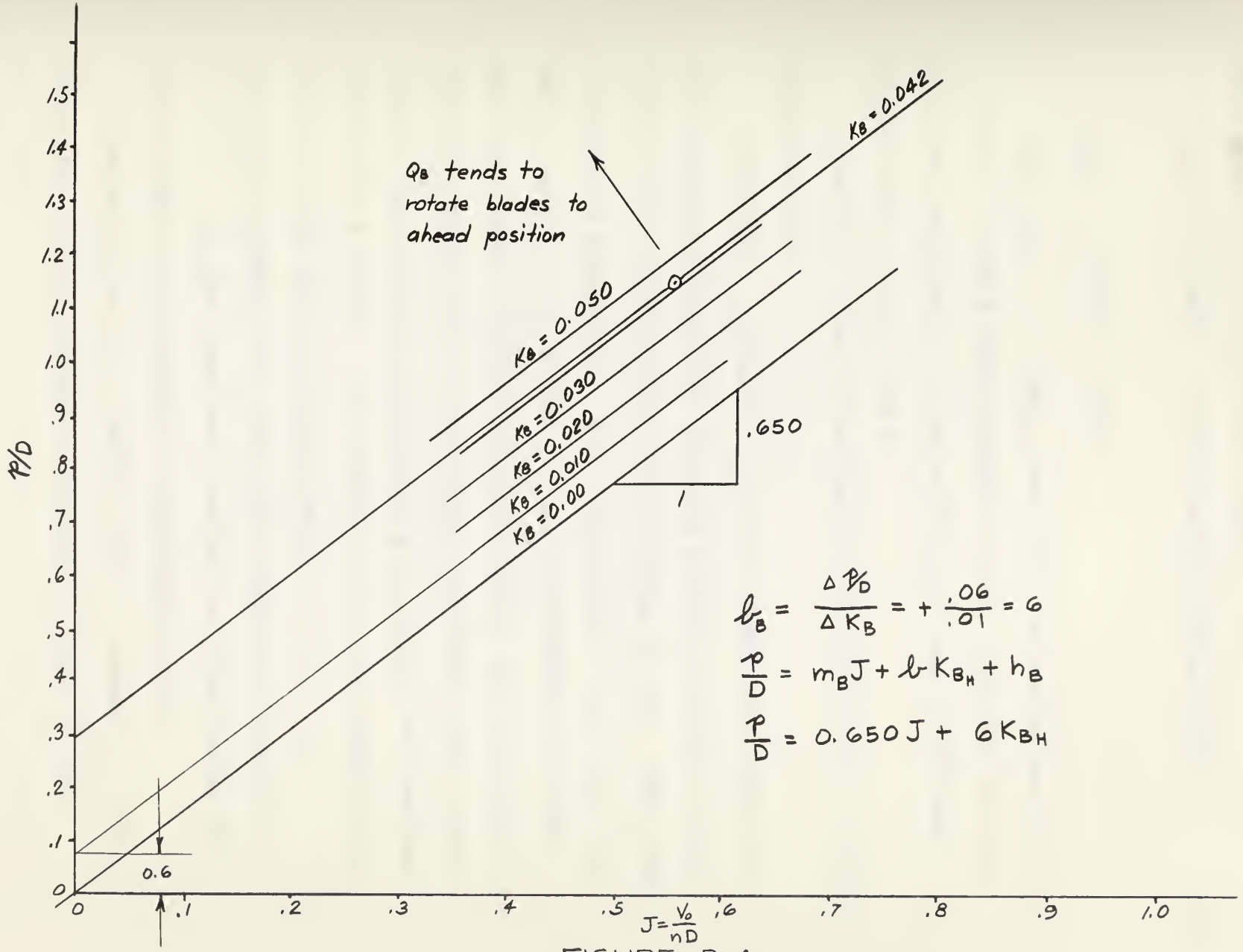

$$b_B = \frac{\Delta P/D}{\Delta K_B} = + \frac{.06}{.01} = 6$$

$$\frac{P}{D} = m_B J + b K_{B_H} + h_B$$

$$\frac{P}{D} = 0.650 J + 6 K_{B_H}$$

FIGURE B-4
Assumed K_B (Hydrodynamic) Curves

coefficient, f, of 0.10, was assumed.

$$Q_{BS} = fr \frac{T_{\perp} \ell N}{b} = \frac{(0.10)(1.14)(9.8\times10^{4})(4.56)^{4}}{(1.4)} \qquad (25)$$

$$Q_{BS} = 1.455\times10^{6} \text{ lb-ft.}$$

Since Q_{BS} is so large, even with low estimates for f, r, l, and $T_{\perp}$ and a high estimate b, the value for sliding friction contributed by the control rod and piston was assumed zero. i.e. $f_R = 0$

A sketch of the hub mechanism with dimensions is shown in Figure B-6.

Reference 11 contains a plot of control rod force for the transient conditions of going from full ahead to full astern while the propeller was spinning in air. This curve is shown in Figure B-7. For a spin test in air the thrust forces causing high values of sliding friction are small. The long region of both transient curves that are parallel with the steady state (centrifugal component only) correspond to the condition of maximum pump output and constant speed of the piston. The deviation from the steady state curve in both cases is approximately 3×10^{4} lbs. Reference 11 states that the total control rod travel is 0.318 ft. and that complete reversal of pitch takes five seconds when the propeller is spinning in air.

Assuming that this entire force is caused by viscous friction, and the maximum ram speed is equal to the

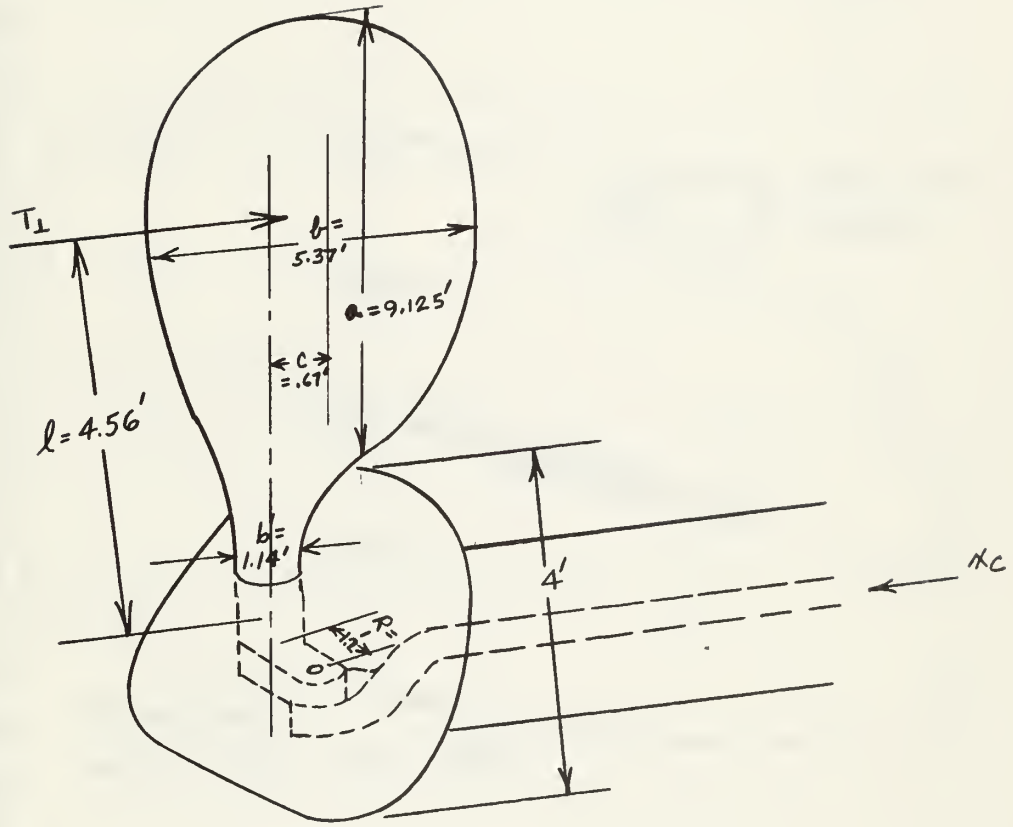

FIGURE B-6

Propeller Mechanisms Showing Only One Blade

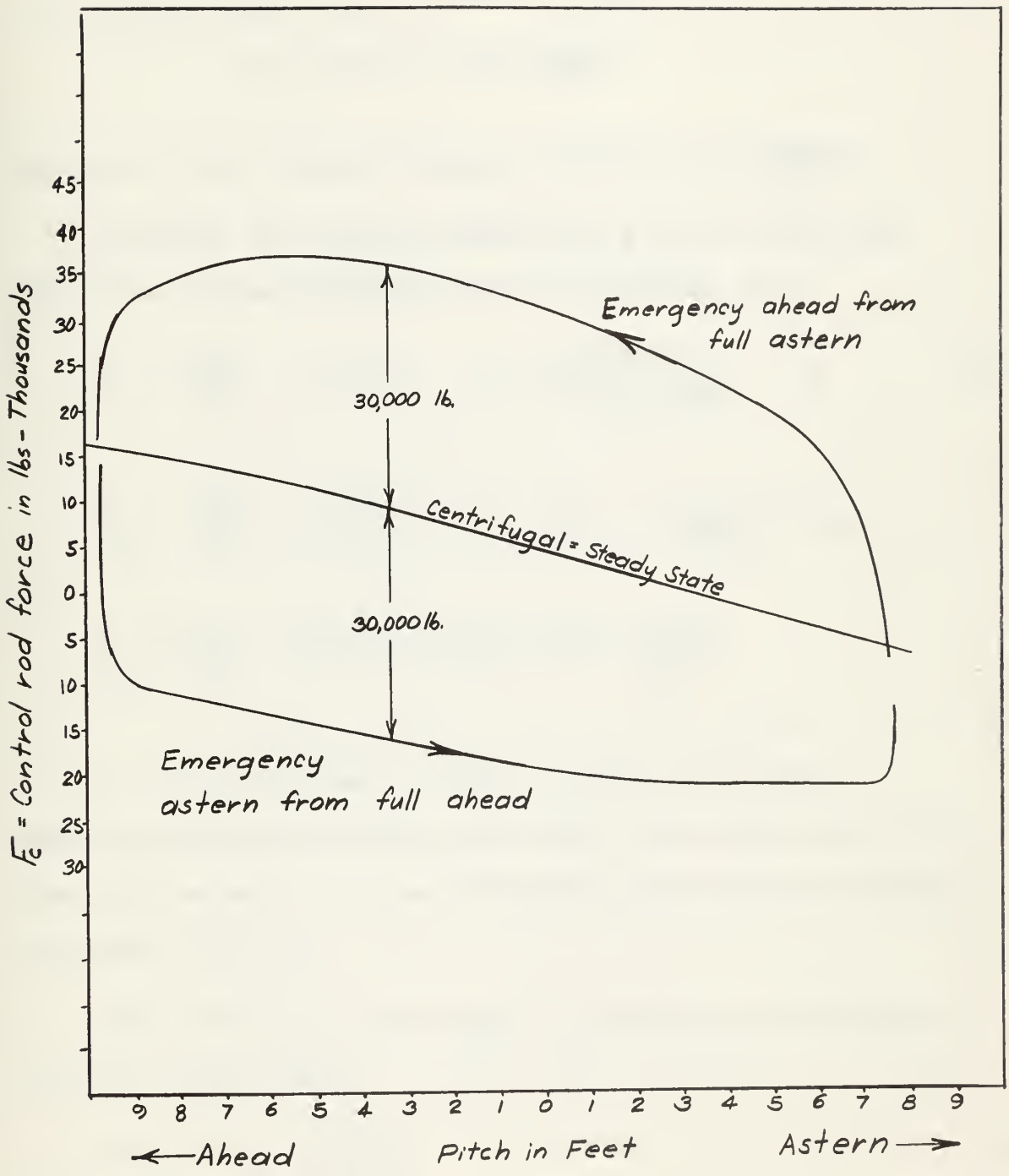

FIGURE B-7

YTB-502 Control Rod Force for Spin Test in Air from Data by Rupp

average speed,

$$\bar{\dot{X}}_c = \frac{.318}{5} = .0636 \text{ ft/sec}$$

the viscous force = 3.0×10^{4} lb = $\mu \bar{\dot{X}}_c$

$$\mu = 4.71 \times 10^5 \frac{\text{lb-sec}}{\text{ft}}$$

where μ = total viscous damping coefficient, $\frac{\text{lb-sec}}{\text{ft}}$

Assuming the viscous forces scale as the area and using the viscous friction term of equation (42),

$$\frac{1}{\pi D}\left(\frac{\alpha_B N}{R} + \mu_R R\right) = \mu \left(\frac{D_{victory}}{D_{YTB\text{-}50}}\right)^2 R \qquad (47)$$

$$\frac{1}{\pi D}\left(\frac{\alpha_B N}{R} + \mu_R R\right) = 4.71 \times 10^5 \left(\frac{18.25}{9.5}\right)^2 1.2$$

$$\frac{1}{\pi D}\left(\frac{\alpha_B N}{R} + \mu_R R\right) = 3.65 \times 10^5 \frac{\text{lb-sec}}{\text{ft}}$$

In order to obtain a value for the polar mass moment of inertia of the blade about its spindle axis, the blade is assumed to be an elliptical plate with an average thickness = $\frac{1}{6}$ ft.

The formula for the moment of inertia of an ellipse about its major axis:

$$J_{iBb} = t\rho_P \frac{a^{3/2} b \pi}{8\sqrt{2}} \qquad (48)$$

where t = thickness of plate, ft.

ρ_P = density of metal, $\frac{\text{lb-sec}^2}{\text{ft}^3\text{-ft}}$

a = length of minor axis, ft.

b = length of major axis, ft.

J_{iBb} = mass moment of inertia of blade about major axis, lb-ft-sec^2

The axis of the spindle is offset so that approximately 40% of the area is forward of the spindle axis.

$$\therefore J_{iB}N = t\rho_P \frac{a^{3/2}b\pi N}{2} + C^2 t \rho_P \pi abN$$

where

C = distance of spindle axis from the major axis, ft.

N = number of blades

Substituting values:

$$J_{iB}N = \frac{1}{6}\left(\frac{533}{32.2}\right)\frac{(5.37)(9.125)^4}{8\sqrt{2}} + (.67)^2 \frac{1}{6}\left(\frac{533}{32.2}\right)\pi (5.37)(9.125)4 \qquad (49)$$

$$J_{iB}N = 808.5 \text{ lb-ft-sec}^2$$

Estimating the mass of the control rod a length of 20 feet was assumed.

$$M_c = \rho_c \pi \left(\frac{R_c}{12}\right)^2 L = \frac{492}{32.2}\left(\frac{7.65}{12}\right)^2 (20) = 740 \frac{\text{lb-sec}^2}{\text{ft}}$$

where

ρ_c = mass density of steel, $\frac{\text{lb-sec}^2}{\text{ft}^4}$

R_c = radius of control rod, 7.67 inches

L = rod length, ft.

This is a large estimate for control rod mass, but it is shown in Appendix C that inertia loading can be neglected even for this large estimate.

Allowing a 30% increase for entrained water an estimate of $J'_{iB} = 1050.0$ lb-ftsec^2 is obtained.

The assumption of an elliptical plate was also made in evaluating the constants for centrifugal blade torque, K_{10} and K_{11}.

The formula for an ellipse:

$$\frac{X^2}{a^2} + \frac{Y^2}{b^2} = \frac{1}{4} \quad . \tag{50}$$

Translating the axis to the blade root and solving for X:

$$X = a\left(\frac{1}{4} - \frac{Y^2}{b^2}\right)^{\frac{1}{2}} + \frac{b}{2} \quad . \tag{51}$$

The blade section area, A, is a function of distance from the root, .

$$A = t2X = 2t\left[a\left(\frac{1}{4} - \frac{Y^2}{b^2}\right)^{\frac{1}{2}} + \frac{b}{2}\right] \quad . \tag{52}$$

The distance from the center of the area to the spindle axis in the x direction is assumed constant = c. The distance of the center of the blade section to the spindle axis in the y direction is a function of rake.

$$y = m_r \ell \tag{53}$$

where m_r = slope of blade from vertical.

Substituting equations (52) and (53) into equation (36):

$$K_{10} = N \rho_P \int_{hub}^{tip} Axyd\ell \qquad (36)$$

$$K_{10} = N \rho_P \int_{hub}^{tip} 2t \left[a\left(\tfrac{1}{4} - \frac{Y^2}{b^2}\right)^{\frac{1}{2}} + \frac{b}{2} \right] cm_r \ell \, d\ell$$

If m_r is small the vertical distance is approximately equal to the blade length.

$$K_{10} = N \rho_P \int_{hub}^{tip} 2t \left[a \left(\tfrac{1}{4} - \frac{Y^2}{b^2}\right)^{\frac{1}{2}} + \frac{b}{2} \right] cm_r Y dY \, . \qquad (54)$$

Integrating:

$$K_{10} = N \rho_P \, 4tcm_r a \left[\frac{Y}{2b} \left(\frac{b^2}{4} - Y^2\right)^{\frac{1}{2}} + \frac{b^2}{8b} \, \text{Sin}^{-1}\left(\frac{2Y}{b}\right) \right]_0^{\frac{b}{2}}$$

$$+ N \rho_P 4tcm_r \frac{b}{2} \left[\frac{Y^2}{2} \right]_0^{\frac{b}{2}}$$

Assuming $m_r = \frac{1}{4}$ and substituting values for the remaining variables:

$$K_{10} = 4 \left(\frac{553}{32.2}\right) \left(\frac{4}{6}\right) (.67)\left(\tfrac{1}{4}\right)(2.685) \quad \frac{9.125\,\pi}{(2)(8)(4)}$$

$$+ 4 \left(\frac{553}{32.2}\right) \left(\frac{4}{6}\right)(.67)\left(\tfrac{1}{4}\right) \frac{(9.125)^3}{(64)}$$

$$K_{10} = 105.7 \ \text{lb-ft-sec}^2$$

The formula for the moment of inertia of a rectangle about it centerline:

$$I_{MIN} = \frac{t^3 X}{12} \quad .$$

where the length = X (55)

also

$$I_{MAX} = \frac{(X)^3 t}{12} \tag{56}$$

Using formula (51) for X, the expression for K_{11} can be approximated using equation (37).

$$K_{11} = N \pi D \rho_P \int_{root}^{tip} (I_{MAX} - I_{MIN})\, dY. \tag{37}$$

$$K_{11} = N \pi D \rho_P 2 \int_0^{\frac{b}{2}} \left\{ \frac{\left[a\left(\frac{1}{4} - \frac{Y^2}{b^2}\right)^{\frac{1}{2}} + \frac{b}{2} \right]^3 t}{12} - \frac{t^3}{12} \left[a\left(\frac{1}{4} - \frac{Y^2}{b^2}\right)^{\frac{1}{2}} + \frac{b}{2} \right] \right\} dY \quad . \tag{57}$$

After expanding the cubed term, (57) integrates to

$$K_{11} = \frac{N \pi D \rho_P t a b}{12} \left[\frac{\pi}{64} + \frac{a}{8} + \frac{3b^2}{32} \right]$$

$$- N \pi D \rho_P \frac{t^3 a}{6} \left[\frac{b\pi}{32} \right] - \frac{N \pi D \rho_P t^3 b^2}{24} \tag{58}$$

Expression (58) reduces to

$$K_{11} = \frac{N\pi D\rho_p bt}{768a}\left\{ a^2\left[a^2+\pi(6b^2-3)\right] -32bt^2\right\} \qquad (59)$$

Upon substitution of the limits.

Substituting values for the various parameters:

$$K_{11} = \frac{4\pi\,(18.25)(\frac{553}{32.2})(9.125)(\frac{1}{6})}{768\,(5.37)}\left\{(5.37)^2\left[(5.37)^2 + \pi 6(9.125)^2 - 3\pi\right] -32\,(9.125)(\frac{1}{6})^2\right\}$$

$$K_{11} = 945 \text{ lb-sec}^2$$

3. Pitch Control Mechanism Parameters.

The value for R is obtained from the geometry of the hub mechanism and is shown in Figure B-6 to be about 1.2 ft., which is the maximum feasible for this size propeller.

A maximum operating pressure of 1000 (b/in^2 was assumed.

The piston area required is obtained from summing the forces on the control rod and dividing by the pressure.

Combining equations (21) and (35) and substituting operating point valves for the variables yields the spindle torque cause by hydrodynamic and centrifugal forces.

$$Q_{BH} + Q_{BC} = (K_7 - K_{11})\, p\omega^2 - K_8 V_o \omega - (K_9 + K_{10})\omega^2$$

$$Q_{BH} + Q_{BC} = (482 - 945)(21.0)\,(\frac{10\pi}{3})^2$$

$$\mp 1955\,(16.7)(\frac{10\pi}{3}) - (0 + 105.7)(\frac{10\pi}{3})$$

$$Q_{BH} + Q_{BC} = 1.063 \times 10^7 \text{ lb-ft}$$

when the maximum torque condition prevails.

$$Q_{BS} = \pm \frac{frT_t \ell N}{b} = \frac{(.10)(1.14)(9.8 \times 10^4)(4.56)4}{1.4}$$

$$Q_{BS} = \pm 1.455 \times 10^6 \text{ lb-ft}$$

If these were the only torques to overcome, ie neglecting viscous friction and inertia loading, the total torque would be the sum of the torques above.

$$Q_{BH} + Q_{BC} + Q_{BS} = 1.063 \times 10^7 + 1.455 \times 10^6$$

$$Q_{BH} + Q_{BC} + Q_{BS} = 12.09 \times 10^6 \text{ lb-ft}$$

Dividing by R yields control rod force.

$$\frac{Q_{BH} + Q_{BC} + Q_{BS}}{R} = \frac{12.09 \times 10^6}{1.2} \text{ lb} = 1.005 \times 10^7 \text{ lb}$$

The ram area, A_R, becomes

$$\frac{1.005 \times 10^7 \text{ lb-in}^2}{1000 \text{ lb}} = 1.0 \times 10^4 \text{ in}^2$$

A piston of this size would not fit within the hub of 4 ft. diameter for the Design II type mechanism and is excessively large in any case. Hence a piston area of 775 in^2 is assumed which gives a piston radius of 15.75 in. This size is about the maximum that can be housed within the hub and for either design there is a likelihood of stalling under the heavier load conditions. A larger diameter causes extreme demands on pump output in order to obtain a

reasonable response for the pitch setting mechanism. This pump must be very large even with this size piston.

As is shown in Appendix E, the time constant of the pitch control mechanism is

$$\tau_P = \frac{RA_R}{K_P \pi DM} \tag{60}$$

It is necessary to reduce this time constant to as small a value as possible. The larger this time constant, the less effective the control mechanism becomes in RPM regulation. This is shown graphically in Figure E-6. As τ_P increases the frequency at which the ratio of RPM fluctuation to wake disturbance begins to increase for all systems with regulation decreases.

Higher values of K_P result in lower values of τ_P. The higher values of K_P correspond to large pump capacities. Assuming a 300 H.P. variable displacement is the maximum available K_P is calculated as follows:

A 300 HP variable displacement pump is approximately capable of a maximum delivery of 120,000 in^3/min = 2000 in^3/sec.

The maximum control arm displacement is arbitrary and depends on the length of the lever. A reasonable value for this parameter is 4.368 inches.

Hence,

$$K_P = \frac{2000}{4.368} \frac{in^3}{in\text{-}sec} = 458 \frac{in^3}{in\text{-}sec}$$

The leakage constant, K_L, can be estimated by assuming a maximum % of full pump displacement at full pressure.

$$K_L = \frac{2000 \frac{in^3}{sec}}{1000 \frac{lb}{in^2}} \quad \text{(assumed \%)} \tag{61}$$

$$K_L = 0.2 \frac{in^5}{sec\text{-}lb} \quad \text{for 10\% leakage}$$

$$K_L = 0.02 \frac{in^5}{sec\text{-}lb} \quad \text{for 1\% leakage}$$

The mechanical feedback shown in Figures A-7 and A-10 is determined by the length of linkages e and f or the length and width of the valve port in the case of Design II. Increasing this feedback decreases τ_p, but also decreases the overall pitch mechanism feedback gain as shown in Figures E-4 and E-5. This corresponds to requiring a progressively longer travel of mechanical input at y in Figure A-7 or on A-8. The sensing devices whether tachometers or torquemeters will produce electrical or weak mechanical outputs. A long mechanical travel at y in either case introduces additional time lags that reduce system performance because of inertia loading at a point in the circuit having a low power level. Reasonable values for the linkage lengths were therefore assumed as follows:

e = 5 inches

f = 15 inches

a = 5 inches

b = 5 inches

The G_2 which corresponds to the gain of the stroke piston system is assumed to be one, i.e. it acts purely as a force amplifier.

$$M \equiv \frac{12G_2eR}{(e + f_\ell)\pi D} = \frac{(12)(1)(5)(1.2)}{(5+15)\pi\ (18.25)} = 0.063$$

The time constant for the stroke piston system is smaller than any other time constants in the system by several orders of magnitude and is therefore neglected.[6]

The compliance constant, K_c, is determined from equation (62).

$$K_c = \frac{V}{B} \tag{62}$$

where

V = volume of oil under pressure, in^3

B = bulk modulus of hydralic fluid, $\frac{in^2}{lb}$

$B = 0.27 \times 10^6 \frac{lb}{in^2}$ for standard hydralic oils.

The maximum piston travel is,

$$x_{c_{MAX}} = \frac{Rp}{\pi D} = \frac{(1.2)(21)}{\pi\ (18.25)} = 0.44 \text{ ft.}$$

The volume of oil under compression in the piston is,

---

6. Truxal, J.G., op.cit., p.15-44.

$$A_R \, x_{c_{MAX}} = 0.44 \times 775 \times 12 = 8{,}200 \text{ in}^3$$

Assuming a 10 foot length of piping under compression with a diameter of 3.4 inches, the volume under compression in piping is,

$$(20)(12)\left(\frac{3.4}{4}\right)^2 \pi = 1180 \text{ in}^3$$

The total volume under compression:

$$8{,}200 + 1{,}180 = 9{,}380 \text{ in}^3$$

$$\therefore K_c = \frac{V}{B} = \frac{9380}{0.27 \times 10^6} = .0336 \frac{\text{in}^5}{16}$$

4. Power Plant Characteristics

Propeller inertia (including entrained water), propeller damping, power plant inertia referred to the propeller shaft, and engine damping assuming the turbine is a constant torque device, is taken from Sutton's vibration analysis of the Victory Ship, (AP2).[7]

$$J_{iP}' = 3.09 \times 10^4 \text{ lb-ft-sec}^2$$

$$J_{iE}' = 3.31 \times 10^5 \text{ lb-ft-sec}^2$$

$$\alpha_E = 3.08 \times 10^4 \frac{\text{ft-lb-sec}}{\text{rad}}$$

---

7. A.D. Sutton, "Torsional Vibration of a Geared Turbine Propulsion System." New England Section Paper of the Society of Naval Architects and Marine Engineers, October 1953, p.27.

$$\mathcal{L}_p = 7.54 \times 10^4 \ \frac{\text{ft-lb-sec}}{\text{rad}}$$

$\mathcal{L}_p$ is also found in Appendix E to be equal to K_3^* and can also be determined from propeller curves.

APPENDIX C

Development of the Non-Linear Analogue

The final expressions derived in Appendix A could be programed directly for analogue computation. Simplification of equation (46) greatly reduces the complexity of the program and is therefore desirable.

The compliance term in equation (46) contains

$$\frac{d}{dt}\left\{\frac{(K_7-K_{11})}{R}\, p\omega^2 - \frac{K_8 V_o \omega}{R} - \frac{(K_9+K_{10})}{R}\omega^2 \pm \frac{(f_R + f_r T_\perp \ell N)}{bR}\right\}. \qquad (63)$$

Performing the derivative,

$$\frac{1}{R}\left\{(K_7-K_{11})(\dot{p}\omega^2 + 2\omega p\dot{\omega}) - K_8\dot{V}_o\omega - K_8\dot{\omega}V_o \pm \frac{d}{dt}\left(f_R + \frac{frT_\perp \ell N}{b_R}\right)\right\}$$

ω is the variable being regulated, and even without regulation, $\dot{\omega}$ is small. Therefore, those terms containing $\dot{\omega}$ are assumed zero.

The term $\left(\frac{f_R + f_r T_\perp \ell N}{b}\right)$ is pictured as a function of $\dot{p}$ in Figure C-1.

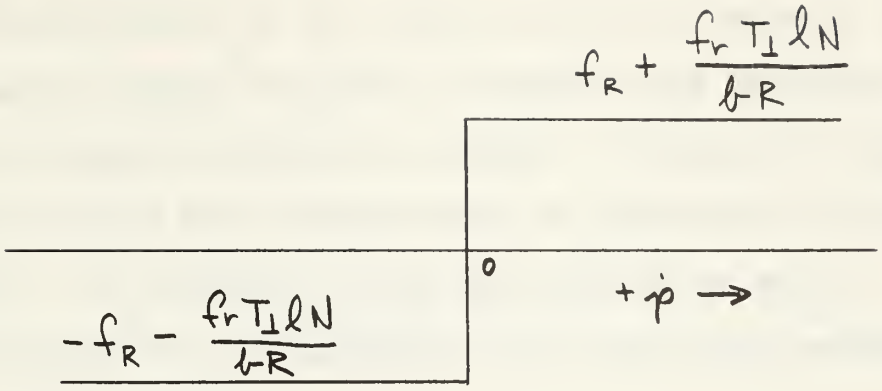

FIGURE C-1

Sliding Friction as a Function of $\dot{p}$

This sliding friction term is discontinuous at $\dot{p} = 0$. The time derivative of the friction term is infinite as the direction of motion of pitch is reversed and therefore causes an impulse of flow or a shock. It does not allow a volume to flow and therefore can be neglected in the analogue. The presence of the term indicates that a hydralic shock will be generated for each pitch reversal in the actual system.

Expression (63) reduces to

$$\frac{1}{R}\left\{ (K_7 - K_{11})\,\dot{p}\omega^2 - K_8\dot{V}_o\omega \right\} \qquad (64)$$

with the above simplications.

Expression (46) contains two terms in $\ddot{p}$. They are

$$\frac{\ddot{p}}{\pi D}\left(\frac{J_{iB}'N}{R} + M_cR\right)\frac{K_L}{A_R} \quad ,$$

and

$$\frac{\ddot{p}}{\pi D}\left(\frac{\alpha_B N}{R} + \mu_R R\right)\frac{K_c}{A_R} \quad .$$

Substituting values into these two terms:

$$\frac{\ddot{p}}{\pi D}\left[\frac{808.5}{1.2} + 740(1.2)\right]\cdot\frac{.0336}{A_R} = \frac{\ddot{p}}{\pi D A_R} \qquad (52.5)$$

and

$$\frac{\ddot{p}}{\pi D}\,(2.08 \times 10^7)\,\frac{2}{A_R} = \frac{\ddot{p}}{\pi D A_R}\,(4.16 \times 10^7) \quad .$$

Hence the first term, envolving inertia and leakage can be neglected.

Substituting expression (47) for expression (46) in equation (37) results in the following three terms containing $\dot{p}$.

$$\dot{p}\,\frac{R}{\pi D}\,A_R = \frac{(1.2)(12)(775)}{\pi(18.25)}\,\dot{p} = 194.9\,\dot{p} \quad in^3/sec$$

$$\dot{p}\,\frac{K_L}{\pi DA_R}\left(\frac{\alpha_B N}{R} + \mu_R R\right) = \frac{(.2)(1.742 \times 10^6)}{(18.25)(775)}\,\dot{p}$$

$$= 0.785\,\dot{p}$$

(For 10% leakage)

$$\dot{p}\,\frac{K_c(K_7-K_{11})\omega^2}{A_R} = \frac{(.0336)(480-945)\left(\frac{10\pi}{3}\right)^2}{775}\,\dot{p}$$

$$= 2.20\,\dot{p} \quad in^3/sec$$

Hence, ignoring these last two terms, equation (46) reduces to:

$$K_P\mu = \dot{p}\,\frac{R}{\pi D}\,A_R + \frac{K_L}{A_R}\left[(K_7-K_{11})\,\frac{p\omega^2}{R} - \frac{K_8 V_o\,\omega}{R}\right.$$

$$\left. -(K_9 + K_{10})\,\frac{\omega^2}{R} \pm \left(\frac{f_R + f r T_\perp \ell\, N}{bR}\right)\right] \qquad (65)$$

$$+ \frac{K_c}{A_R}\left[-\frac{K_8\omega\dot{V}_o}{R} + \frac{\ddot{p}}{D}\left(\frac{\alpha_B N}{R} + \mu_R R\right)\right]$$

Equation (65) and the remaining equations for Design I derived in Appendix A are programed for analogue computation as shown in Figure C-2. Substitution of the parameters determined in Appendix B is shown in Figure C-3.

The analogue computer used will not accept signals of greater than 50 volts. Also, when the output of any amplifier exceeds 50 volts the amplifier response becomes non-linear and saturates completely at about 57 volts. For this reason it was necessary to use the following scales for variables:

pitch, 1 ft = 0.1 volts

shaft speed, 1 $\frac{\text{rad}}{\text{sec}}$ = 0.4 volts

speed of advance, 1$\frac{\text{ft}}{\text{sec}}$ = 0.1 volts

A scale larger than this saturates the path containing $p\omega^2$ terms.

Care must be taken when using different scales for variables when non linear elements such as the multipliers are used.

The general rule for multipliers is to divide the amplification following the multiplier by the product of the two scale factors of the input variables.

Scaling through linear elements such as amplifiers and integrators is accomplished by increasing the coefficient for each input path containing pitch and speed of advance as a variable by a factor of four.

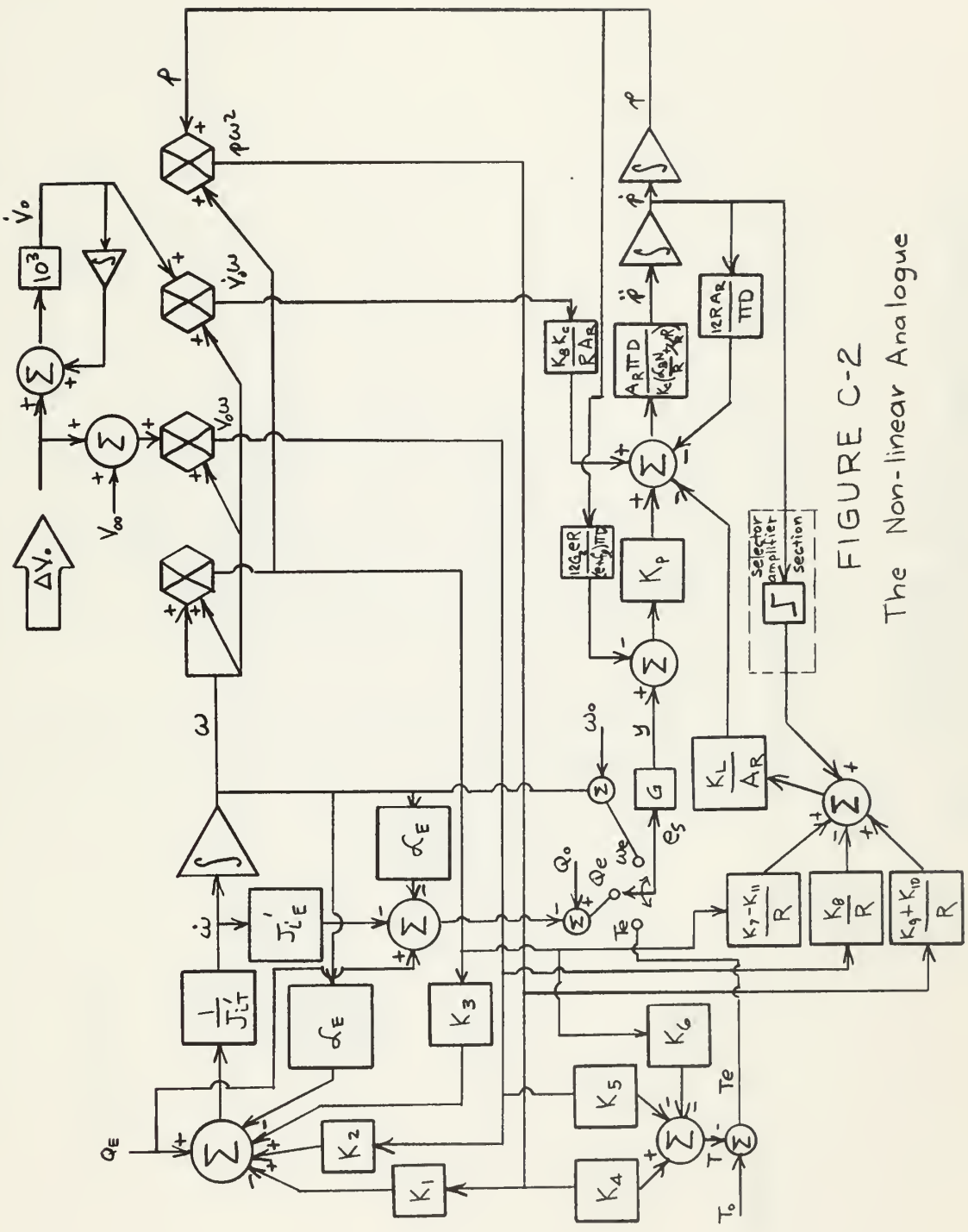

FIGURE C-2

The Non-linear Analogue

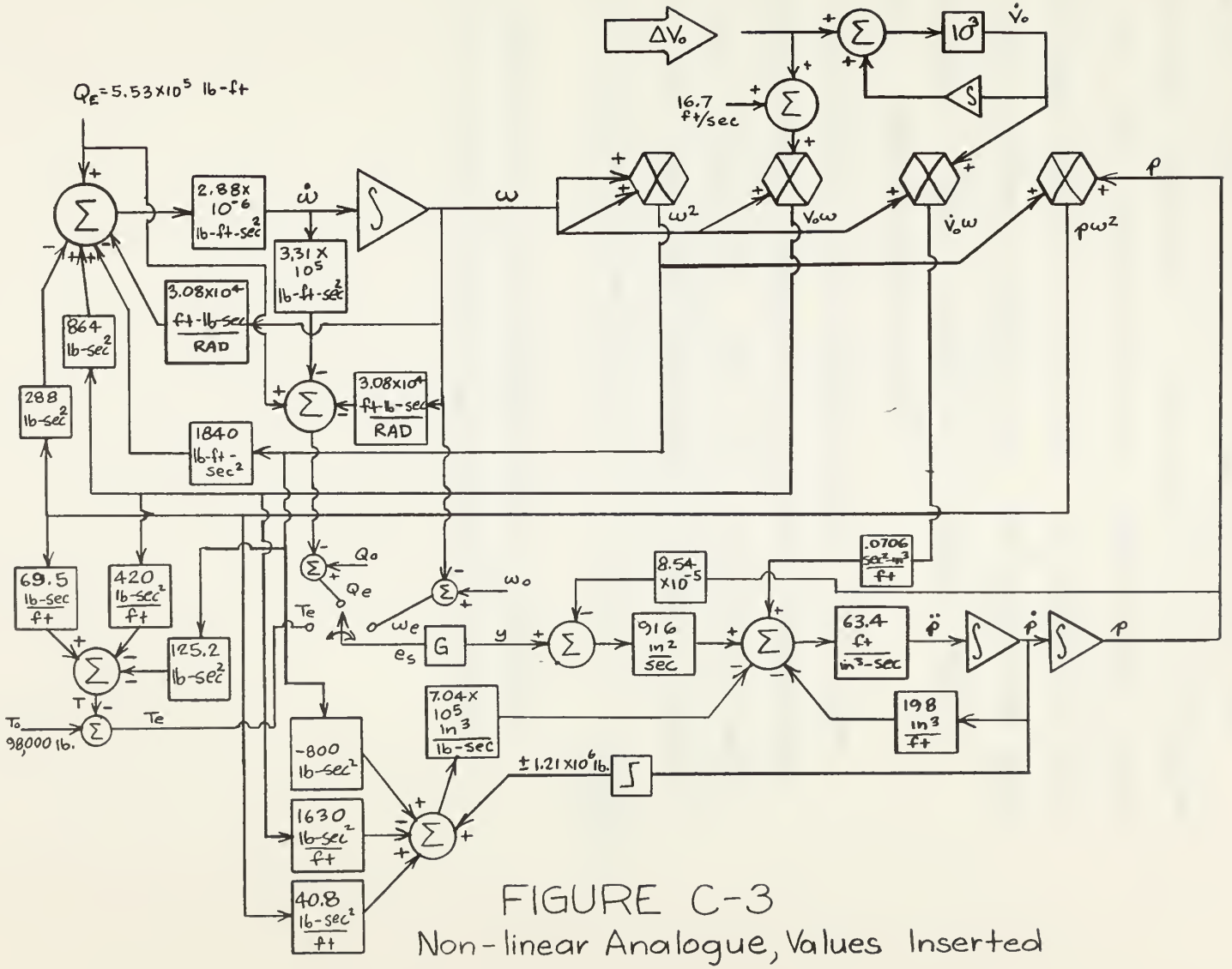

FIGURE C-3

Non-linear Analogue, Values Inserted

Finally it is necessary to move various gains around the system, following the rules of block diagram transformation, so that individual amplifiers will not saturate and the inputs to each amplifier do not exceed four, all with coefficients having their decimal point within three digits of each other. An example of this last step is shown in Figure C-4. The gains must also be arranged so that no amplifier is called upon to provide a gain greater than 10^3.

The portion of the analogue marked "Selector-Amplifier Section" effectively produces the response pictured in Figure C-1. The bias and amplifier gains are set for a very small sinusoidal input to give the correct voltages corresponding to the term, $\left(f_R + \frac{f_r T_1 \ell N}{b_R}\right)$.

Figure C-6 is the analogue with all scaling completed and the program ready for the computer.

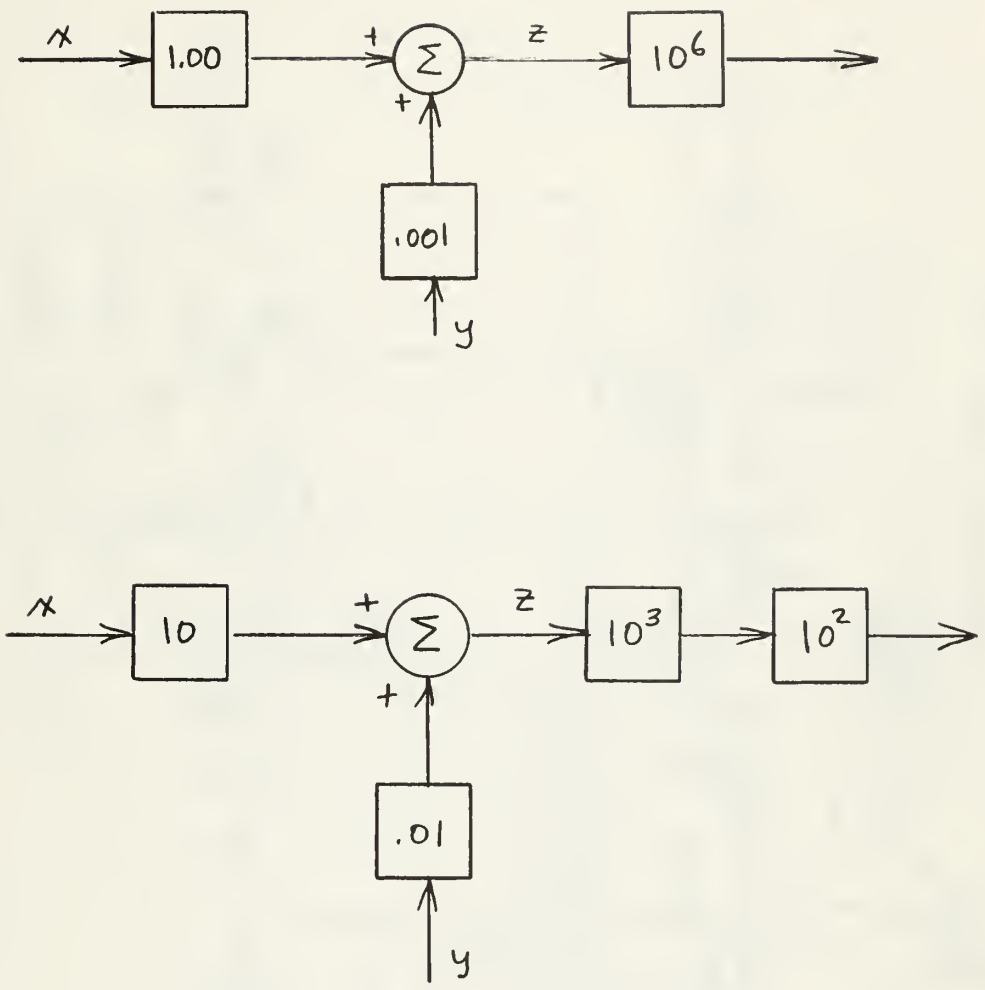

FIGURE C-4

Example of a Block Diagram Transformation

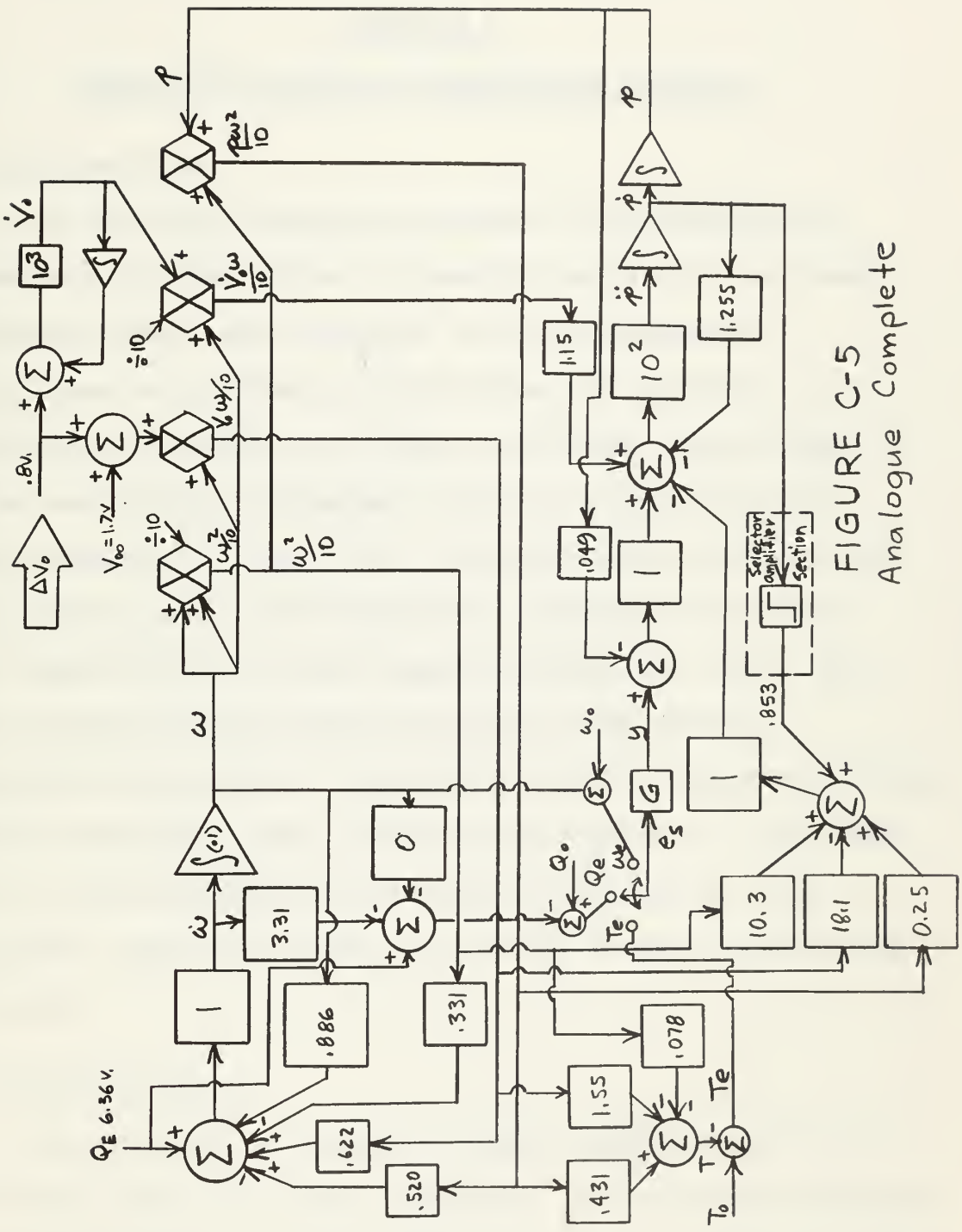

FIGURE C-5
Analogue Complete

APPENDIX D

Non-Linear Analogue Computation Results

1. Difficulties.

The Philbrick Analogue Computer of the Mechanical Department Systems Project Laboratory at M.I.T. was used to obtain data. This computer utilizes electronic multipliers to perform multiplication and division. The multipliers produced a hum that was within the band pass of the amplifiers. Although correct average values for the variables, ω^2, $V_o\omega$, $\dot{V}_o\omega$, and $p\omega^2$ were obtained, the hum superimposed on the signal was transmitted through each amplifier and in some cases obscured the data. The power plant-propeller system and the pitch control mechanism were operated separately with satisfactory results, but the connecting link, marked G in Figure C-2 introduced hum for the variable $\ddot{p}$ saturating the integrator that followed. For this reason, no overall system response was obtained.

2. Useful Results.

The response of the power plant-propeller system to a sinusoidal input of V_o was obtained. A two channel Sanborn recorder was used with the input, V_o, on one channel and the

ω response on the other. The Sanborn recorder stylus deflection was calibrated against a computer amplifier. Each amplifier has a provision for adding up to $\pm$ 50.0 volts to the output in increments of 0.1 volts. With one volt per cm. deflection the recorder output was linear over $\pm$ 2 cm. The maximum output recorded was $\pm$ 2.2 cm. and the accuracy of readings is approximately 0.1 cm. The results are shown in Table D-1 and are plotted in Figure E-6.

The time constant of the power plant-propeller system was observed to be approximately 3.28 sec. This was determined by injecting a step of Q and observing the response in ω. The decay to steady state in ω occured in about 10 sec. or three time constants.

The values of Q_B and Q_P generated had an average value within 5% (3.1 volts and 7.0 volts respectively) of the calculated values at the operating point, but a sinusoidal hum of volts was superimposed on both.

The node corresponding to the variable $\dot{p}$ had a sinusoidal amplitude of .6 volts for a 8 volt sinusoidal input for V_o with no friction feedback. With friction added this signal was reduced to less 0.1 volts (the approximate level of noise). This is an indication of the importance of the strong stabilizing effect of sliding friction.

The feedforward path containing $\hat{V}_o \omega$ had no effect on $\ddot{p}$ even with an input of 30 volts for ΔV_o.

TABLE D-1

Power Plant-Propeller System Frequency Response

frequency cycles/sec	ΔV_o Input (Volts)	$\Delta\omega$ Output (Volt Sx$\frac{1}{4}$)	$\left\lvert\frac{\Delta\omega}{\Delta V_o}\right\rvert$	$10\log_{10}\left\lvert\frac{\Delta\omega}{\Delta V_o}\right\rvert$
0	3.0	0.15	0.050	- 13.0
.01	3.0	0.15	0.050	- 13.0
.02	3.0	0.15	0.050	- 13.0
.03	3.0	0.20	0.066	- 11.8
.04	3.0	0.20	0.066	- 11.8
.05	3.0	0.20	0.066	- 11.8
.06	3.0	0.20	0.066	- 11.8
.07	3.0	0.20	0.066	- 11.8
.08	3.0	0.20	0.066	- 11.8
.09	4.0	0.20	0.050	- 13.0
.1	4.0	0.20	0.050	- 13.0
.2	8.0	0.38	0.048	- 13.2
.3	11.0	0.62	0.056	- 13.4
.4	15.0	0.84	0.056	- 13.4
.5	18.0	0.79	0.044	- 13.5
.6	24.0	1.03	0.043	- 13.6
.7	26.0	1.10	0.042	- 13.7
.8	28.0	1.16	0.0415	- 13.8
.9	30.0	1.25	0.0415	- 13.8
1.0	38.0	1.52	0.0400	- 14.0
2.0	38.0	1.45	0.0380	- 14.2
3.0	38.0	1.0	0.0264	- 15.8
4.0	38.0	0.50	0.0130	- 18.8
5.0	40.0	0.00	0	- ∞

APPENDIX E

Linear Incremental Analysis

1. Simplification of the model equation (46) contains the term,

$$\frac{12G_2\, eRK_p}{(e + f_\ell)\pi D} ,$$

which is mechanical feedback.

Define $$\frac{12G_2 eR}{(e + f_\ell)\pi D} \equiv M \qquad (66)$$

As shown in Appendix C, a reasonable value for this term is

$$M = 0.063 \quad .$$

As shown in Appendix D, the terms $\frac{\ddot{p}}{\pi D}\left(\frac{\alpha_B N}{R} + \mu_R R\right)\frac{K_c}{A_R}$, and $\frac{K_L}{A_R}\ \frac{K_8 V_o \omega}{R}$, are small in comparison to the remaining terms of equation (45). Neglecting these terms the analogue for the pitch setting mechanism, as shown in Appendix B, can be reduced to that shown in Figure E-1. This is equivalent to neglecting the corresponding term of equation (46), which reduces to

$$\dot{p} = \frac{1}{\frac{R}{\pi D} A_R} \left\{ K_p x - \frac{K_L}{A_R}\left[(K_7 - K_{11})\frac{p\omega^2}{R} - \frac{K_8 V_o}{R} \right.\right.$$

$$\left.\left. -(K_9 + K_{10})\frac{\omega^2}{R} \mp \left(f_R + \frac{f_r T_1 \ell\, N}{b_R}\right) \right. \right. \qquad (67)$$

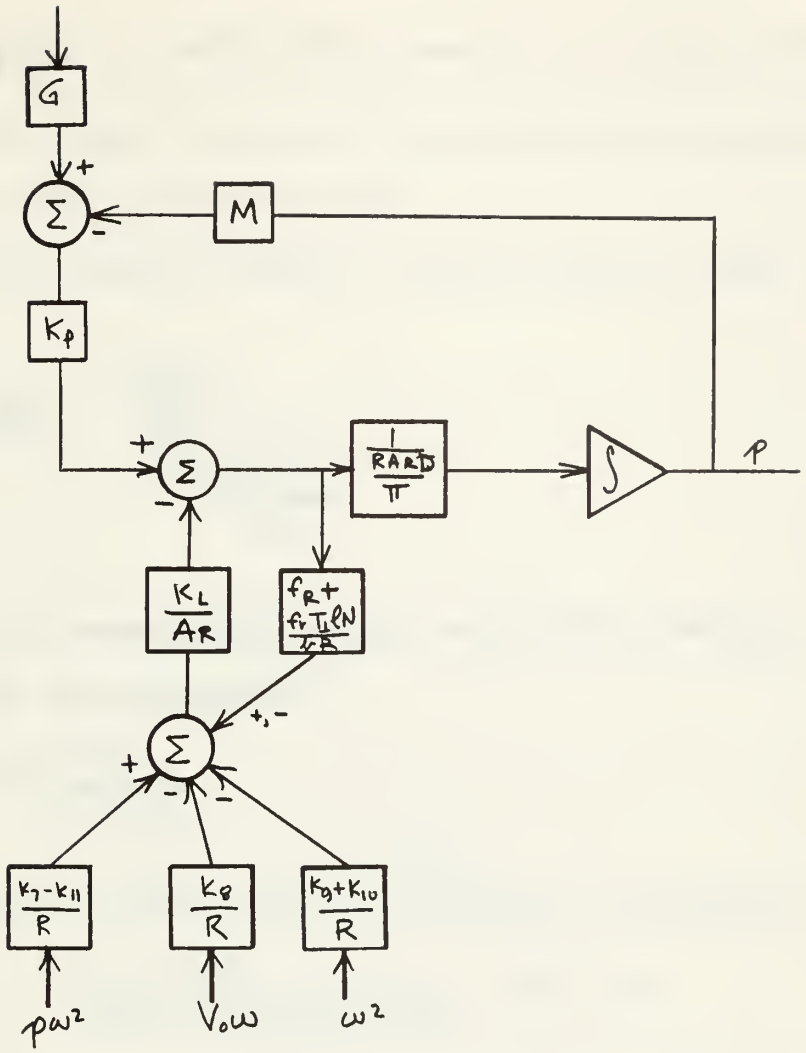

FIGURE E-1

Simplified Pitch Control Analogue

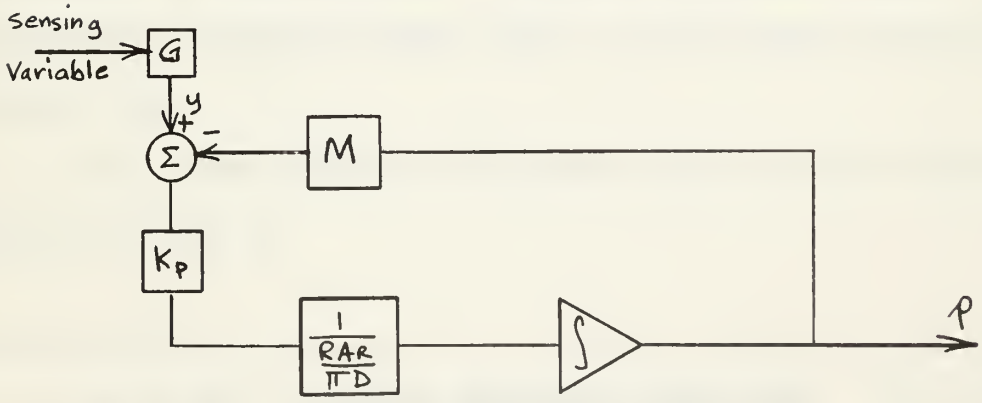

FIGURE E-2

Pitch Mechanism Analogue Neglecting Leakage

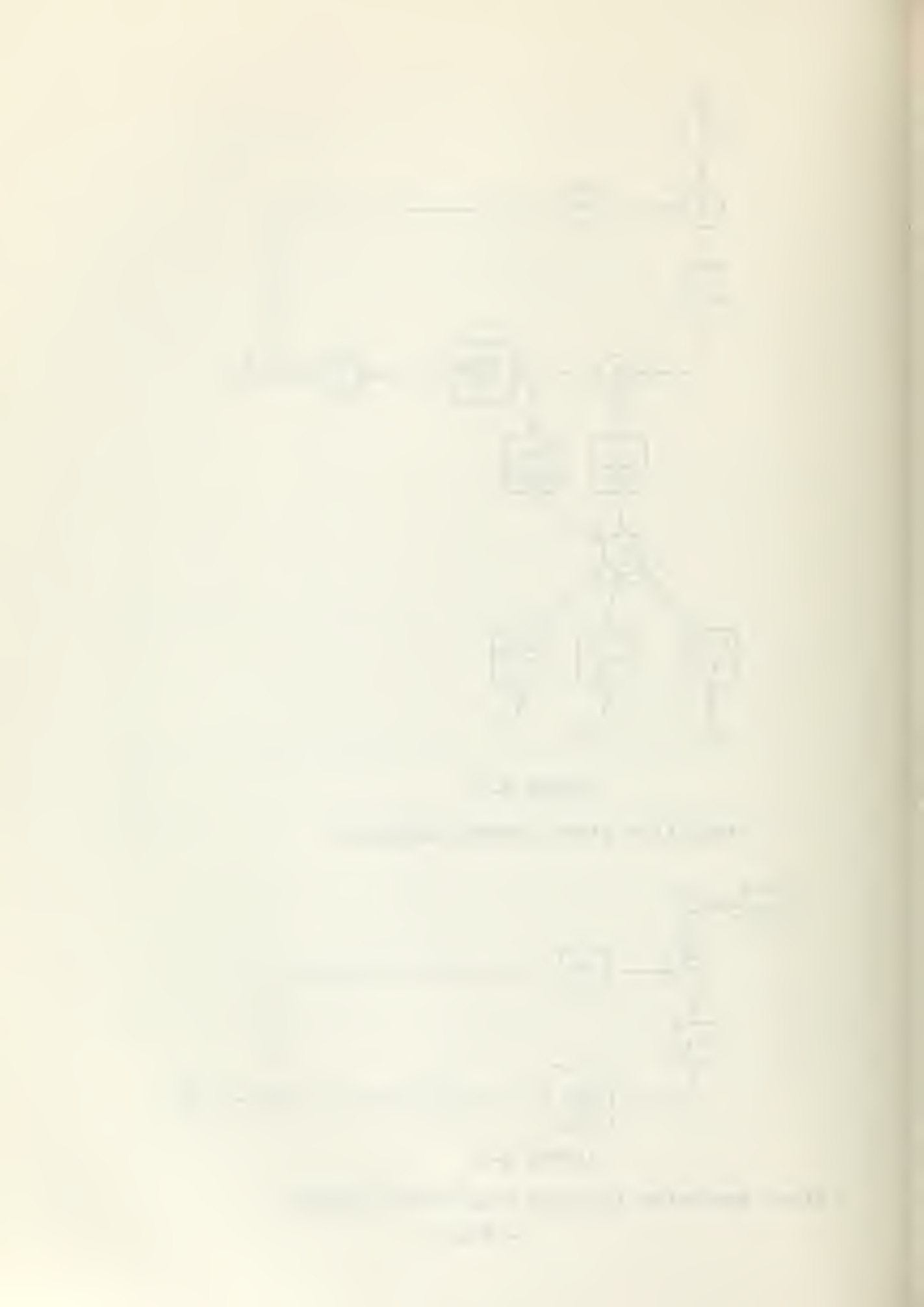

If $\frac{K_L}{A_R}$ is sufficiently small the leakage feedback shown in Figure E-1 can be neglected and the system reduces to that shown in Figure E-2.

The transfer function for the system shown in Figure E-2 is

$$\frac{p'(s)}{y'(s)} = \frac{\frac{K_p \pi D}{RA_R}}{S + \frac{K_p \pi DM}{RA_R}} \tag{68}$$

This constitutes a type zero system having a simple lag with time constant.[8]

$$\tau_p = \frac{RA_R}{K_p \pi DM} \tag{69}$$

Substituting values determined in Appendix C,

$$\tau_p = \frac{(1.2)(775)}{(458)\pi(18.25)(.063)} = .563 \text{ sec.}$$

Leakage has the effect of reducing this time constant. The two largest contributors are friction and the pitch component of blade torque. Figure E-3 shows these additional feedback paths added to the system shown in Figure E-2.

The system transfer function that includes the $p\omega^2$ feedback term is

---

8. J.G. Truxal, Control Engineers Handbook. The Maple Press Co., York, Pa. 1958, p.2-35.

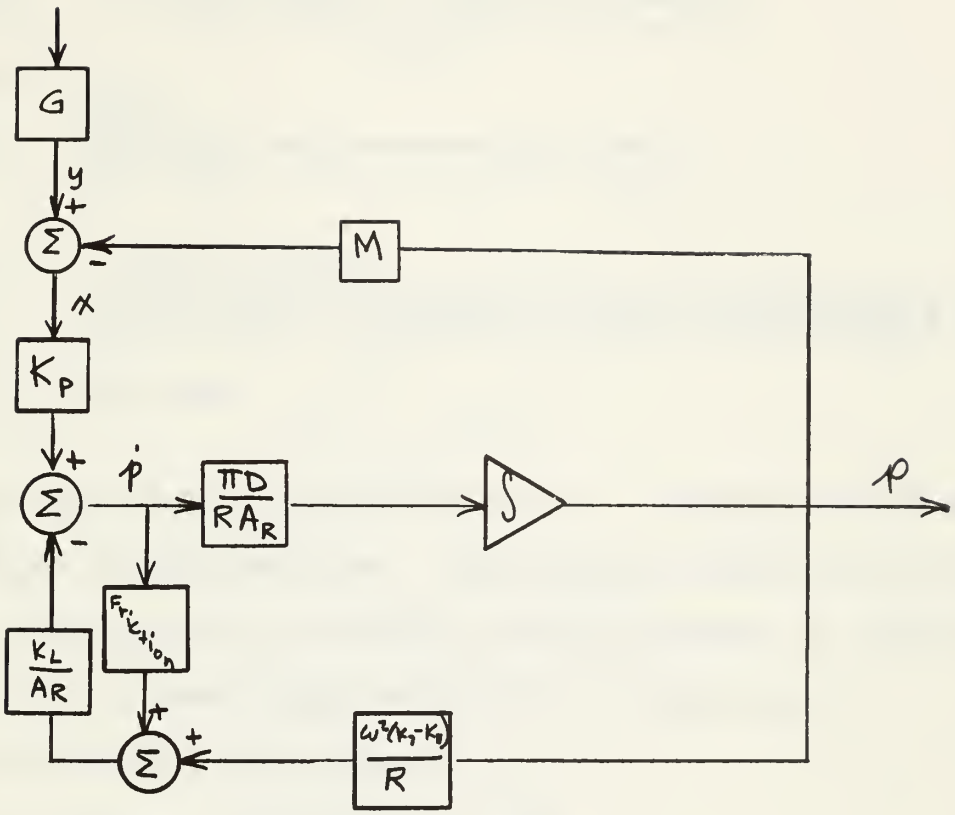

FIGURE E-3

Pitch Mechanism Analogue With Major Leakage Factors Included

$$\frac{P'(s)}{y'(s)} = \frac{\frac{K_P \pi D}{A_R R}}{S + \frac{K_P M \pi D R A_R + (K_7 = K_{11}) \pi D \omega^2 K_L}{A_R^2 R^2}} \quad , \qquad (70)$$

and now,

$$\tau_P = \frac{A_R^2 R^2}{K_P M \pi D R A_R + (K_7 - K_{11}) \pi \omega^2 K_L D} \qquad (71)$$

$$\tau_P = \frac{(775)^2 (1.2)^2}{(458)(.063)\ \pi\ (18.25)(1.2)(775) + (276-482)\pi \left(\frac{10}{3}\right)^2 (18.25)(2)}$$

$$\tau_P = 0.541 \text{ sec.}$$

The computation above is based on a leakage of 10% of pump output at maximum flow. The leakage caused by friction can be approximated as reducing the pump output or effectively reducing K_P as shown diagramatically in Figure E-4.

The effective K_P becomes:

$$K_P' = \frac{K_P x_{max} - \left(f_R + \frac{fr\, \ell\, NT_1}{br}\right) \frac{K_L}{A_R}}{x_{MAX}} \qquad (72)$$

$$K_p' = \frac{(458)(4.368) - (1.210 \times 10^6) \frac{.2}{775}}{(4.368)}$$

$$K_p' = 384 \frac{\text{in}^3}{\text{in-sec}}$$

The new τ_P becomes

$$\tau_P = \frac{RA_R}{K_P' \pi D M} = \frac{(1.2)(775)}{(384)\pi (18.25)(0.63)} \qquad (73)$$

$$\tau_P = 0.654$$

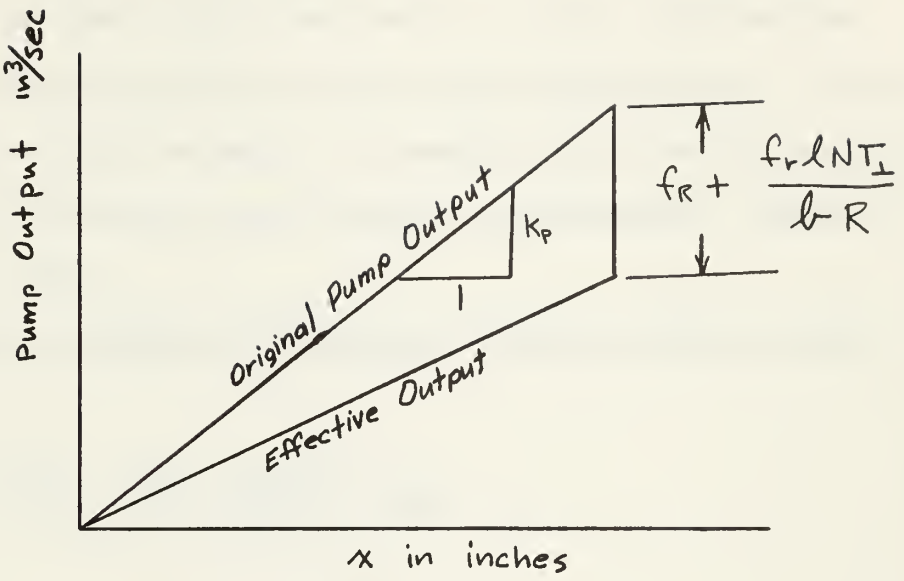

FIGURE E-4

Effect of Leakage on K_p

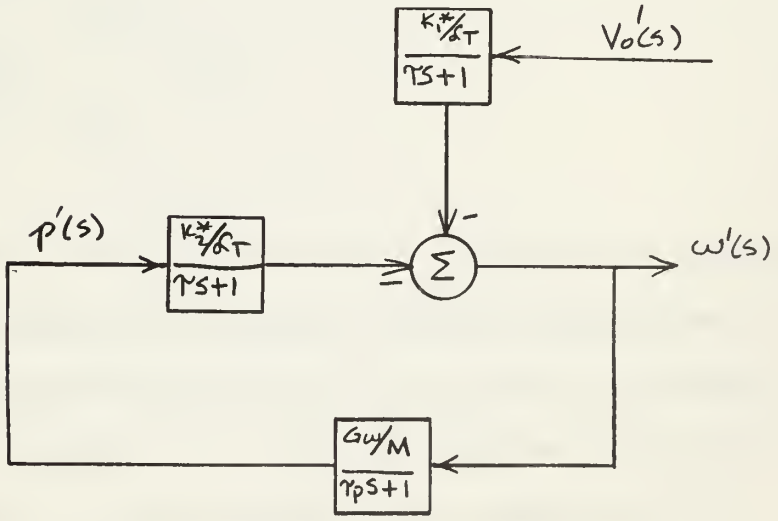

FIGURE E-5

Regulation by ' Sensing

The bad effect of increasing τ_p is shown in the gain plot of Figure E-6. As τ_p increases, the gain defined as the ratio of shaft speed variation to make fluctuation increases and at progressively lower frequencies. It is expected that 10% leakage is excessive and the τ_p computed for 1% will be used in all future calculations. That is

$$\tau_p = 0.560 \quad .$$

Viewing propeller torque as a linear function of p, ω, and V_o,

$$Q_p = K_1^* V_o + K_2^* p + K_3^* \omega + Q_{PO} \tag{74}$$

where

Q_{PO} = operating point torque, ft-lb

$$K_1^* = \frac{\partial Q_p}{\partial V_o}\bigg|_{p,\omega} \tag{75}$$

$$K_2^* = \frac{\partial Q_p}{\partial p}\bigg|_{V_o,\omega} \tag{76}$$

$$K_3^* = \frac{\partial Q_p}{\partial \omega}\bigg|_{V_o,p} = \alpha_p \tag{78}$$

Values for the above K*'s are obtained from propeller curves by allowing the variable in the denominator of the partial derivatives vary over $\pm$ .1 of their operating value, obtaining the K_Q at each of the two points and solving for the Q_p and dividing the result by 0.2.

Calculations for K_1^*, K_2^*, and K_3^*, using Troost's

B4-55 propeller follow:

$$K_1^* = \frac{\Delta Q_P}{\Delta V_o} = \frac{(\Delta K_Q)\rho n^2 D^5}{(.2)nD} \tag{79}$$

$$\Delta K_Q = K_Q \text{ (for } J = 1.1J_o) - K_Q \text{ (for } J = 0.9J_o)$$

where J_o is the operating point advance coefficient.

$$\therefore K_1^* = \frac{(-.007)(1.024)(\frac{10}{6})^2(18.25)^5}{(12)(\frac{10}{6})(18.25)} = -6610 \text{ lb-sec},$$

$$K_2^* = \frac{\Delta Q}{\Delta p} = \frac{(\Delta K_Q)\rho n^2 D^5}{(.2)\ \frac{p}{D} \times D} \tag{80}$$

where $\Delta K_Q = K_Q$ (for $\frac{p}{D} = 1.1\ (\frac{p}{D})_o$)

$$- K_Q \text{(for } \frac{p}{D} = 0.9\ (\frac{p}{D})_o)$$

$$K_2^* = \frac{(.02)(1.024)(\frac{10}{6})^2(18.25)^4}{(.2)(1.15)} = 2.96 \times 10^4 \text{ lb.}$$

$$K_3^* = \frac{\Delta Q}{\Delta \omega} = \frac{(\Delta K_Q)\ \rho\ n^2 D^5}{\Delta n\ 2\pi}$$

In this case p/D and V_o remain constant
but $J = \frac{V_o}{nD}$ changes as $n = \frac{\omega}{2\pi}$ changes by $\pm$ 0.1.

$$K_3^* = \frac{(.006)(1.024)(\frac{10}{6})^2(18.25)^5}{(.2)(\frac{10}{6})\ 2\pi} = 7.54 \times 10^4 \ \frac{\text{ft-lb-sec}}{\text{rad.}}$$

In summary:

$K_1^* = -6610$ lb-sec

$K_2^* = 2.96 \times 10^4$ lb

$K_3^* = 7.54 \times 10^4 \ \frac{\text{ft-lb-sec}}{\text{rad.}}$

Using primes (') to indicate incremental quantities, equation (74) is incrementally,

$$Q_P' = K_1^* V_o' + K_2^* P' + K_3^* \omega \tag{81}$$

From equation (10),

$$-\alpha_E \omega - (K_1^* V_o' + K_2^* p' + K_3^* \omega) = J_{iT}' \dot{\omega}' \tag{82}$$

or using the Laplace transform,

$$\omega'(s)\left[(\alpha_E + \alpha_P) + J_{iT}' S \right] = K_2^* p'(s) + K_1^* V_o'(s) \tag{83}$$

$$\omega'(s) = -\frac{K_2^* P'(s) + K_1^* V_o'(s)}{(\alpha_E + \alpha_P) + J_{iT}' S} \tag{84}$$

The block diagram for which is shown in Figure E-3

2. Shaft Speed Sensing

Sensing angular velocity and adding the pitch setting mechanism to the diagram of Figure E-3 is shown in Figure E-5.

Define: $\alpha_T = \alpha_E + \alpha_P = 3.08 \times 10^4 + 7.54 \times 10^4 = 10.62 \times 10^4 \ \frac{\text{ft-lb-sec}}{\text{rad.}}$

$$\tau = \frac{J_{iT}'}{\alpha_E + \alpha_P} = \frac{3.48 \times 10^5}{10.62 \times 10^4} = 3.28 \text{ sec.}$$

G_ω = gain for angular speed sensing

The transfer function between $V_o'(s)$ and $\omega'(s)$ is:

$$\frac{\omega'(s)}{V_o'(s)} = \frac{-\frac{K_1^*}{\alpha_T}(1-\tau_p S)}{(\tau S+1)(\tau_p+1) + \frac{K_2^* G\omega}{\alpha_T M}} \qquad (85)$$

The selection of G_ω is usually based on criteria for transient response or stability. As G_ω increases the effectiveness of regulation improves for lower frequencies but more severe peaking occurs near resonance. A compromise value of G_ω giving a damping factor, $\xi = 0.4$ was chosen and used as the criteria for ω and Q_S sensing designs. A G_ω giving a damping factor of one provides essentially no improvement of regulation overthe fixed pitch system.

The damping factor is defined for the transfer function when the denominator is placed in the form:

$$S^2 + 2\xi\omega_n S + \omega_n^2 \qquad (86)$$

where

ξ = damping factor

ω_n = natural undamped frequency, sec^{-1}

Placing the denominator of equation (85) in the form of expression (86), and solving for G_ω and ω_n with $\xi = 0.4$

yields:

$$G_\omega = \frac{(\tau_\varepsilon + \tau_p)^2 \alpha_E M}{\tau_\varepsilon \tau_p (.64) K_2^*} = \frac{(3.28+.560)^2 (3.08\text{x}10^4)(.063)}{(3.28)(.560)(.64)(2.96\text{x}10^4)}$$

$$= 0.82 \ \frac{\text{ft-sec}}{\text{rad}} \qquad (87)$$

$$\omega_n = \frac{K_2^* G}{\alpha_\varepsilon \tau_E \tau_p M}^{\frac{1}{2}} = \frac{2.96 \times 10^4 \ (.82)}{(3.08 \times 10^4)(.560)(3.28)(.063)}$$

$$= 2.61 \ \text{sec}^{-1} \qquad (88)$$

System response for angular speed sensing is plotted in Figure E-6.

3. Torque Sensing

If a torquemeter were used in lieu of a tachometer for sensing, regulation of shaft torque might be accomplished. This in turn would regulate shaft angular speed.

Figure E-7 shows the block diagram for the system using torque sensing.

The V_o' to ω' transfer function is now

$$\frac{\omega'(s)}{V_o'(s)} = \frac{\frac{K_1^*}{\alpha_T}(\tau_p S+1)}{S^2 + \left(\frac{\tau_p + \tau \frac{+K_3^* \tau_p}{\alpha_T} + \frac{K_2^* G_Q \tau}{M}}{\tau \tau_p}\right) S + \left(1 + \frac{K_3^*}{\alpha_T} + \frac{K_2^* G_Q}{M}\right)} \qquad (89)$$

Using the same criteria of $\zeta = 0.4$ in the setting of G_Q leads to a quadratic equation in G_Q.

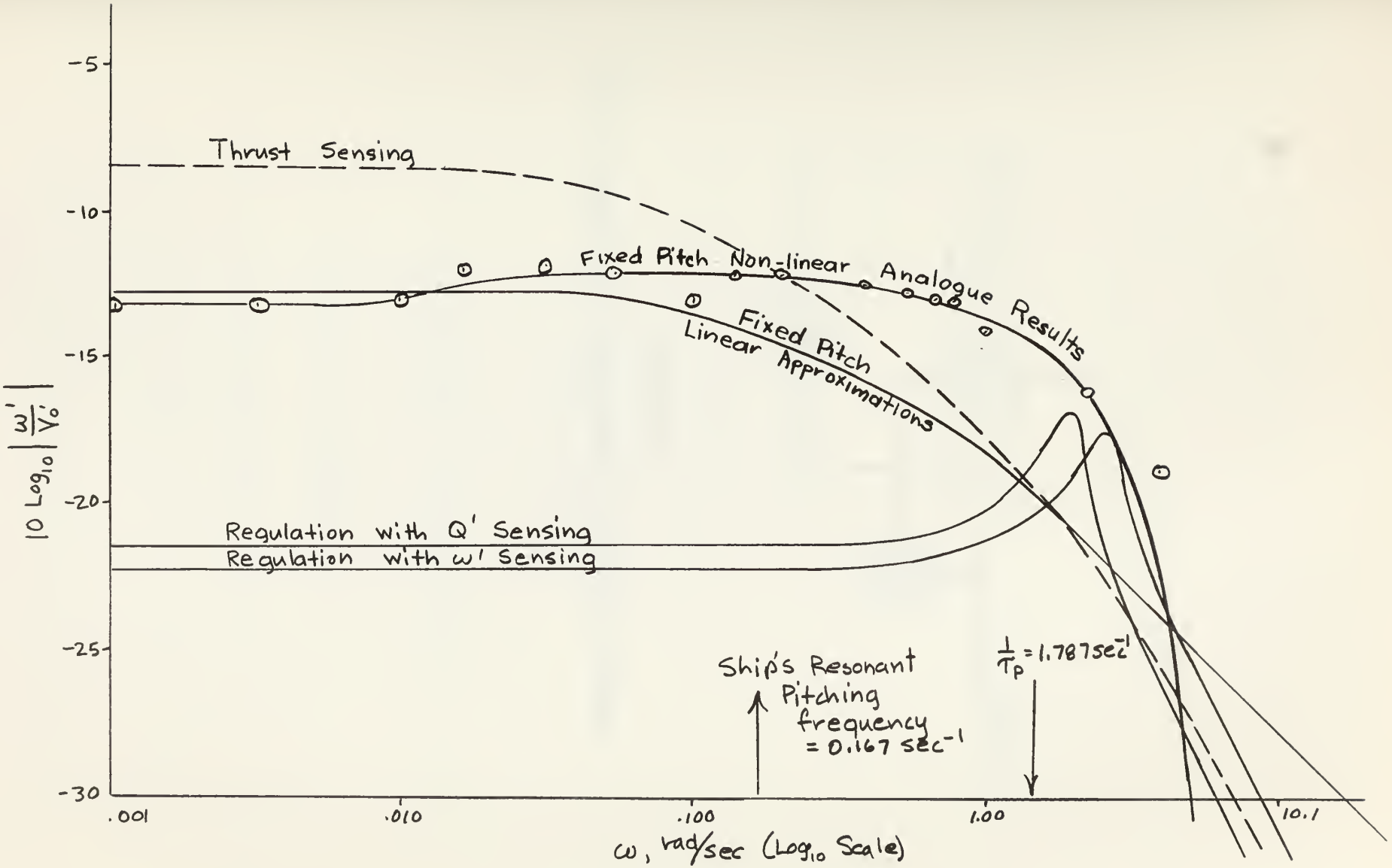

FIGURE E-6

Decilog Plot of Gain for Various Methods of Regulation

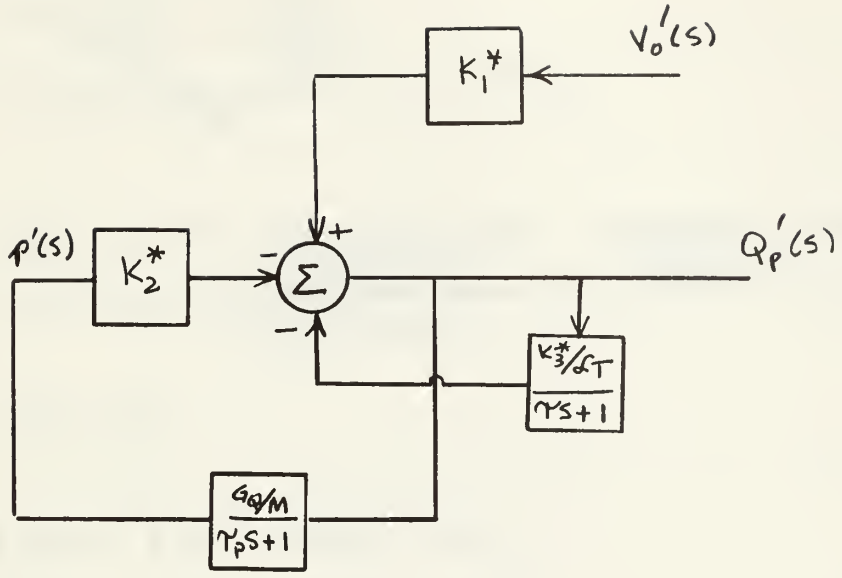

FIGURE E-7

Block Diagram for Regulation by Torque Sensing

Solution for G_Q follows:

From expression (89),

$$\frac{\tau_P+\tau+\frac{K_3^*\tau_P}{\mathcal{L}_T}+\frac{K_2^*G_Q\tau}{M}}{\tau\tau_P}=2\omega_n\xi \quad . \tag{90}$$

$$\frac{.560+3.28+\frac{7.54\times10^4(.563)}{10.62\times10^4}+\frac{2.96\times10^4G_Q(3.28)}{.063}}{(.563)(3.28)}$$

$$=2(.4)\omega_n$$

$$2.301+8.35\times10^5G_Q=.8\omega_n$$

$$2.88+1.042\times10^6G_Q=\omega_n \tag{91}$$

also,

$$\omega_n=\left(1+\frac{K_3^*}{\mathcal{L}_T}+\frac{K_2^*G_Q}{M}\right)^{\frac{1}{2}}\left(\frac{1}{\tau\tau_P}\right)^{\frac{1}{2}} \tag{92}$$

$$\omega_n=\left(1+\frac{7.54\times10^4}{10.62\times10^4}+\frac{2.96\times10^4G_Q}{.063}\right)^{\frac{1}{2}}\left(\frac{1}{3.26\times.560}\right)^{\frac{1}{2}} \tag{93}$$

$$\omega_n=(1.708+4.70\times10^5G_Q)^{\frac{1}{2}} \tag{94}$$

Combining expressions (91) and (94),

$$1.708+4.70\times10^5G_Q=(2.88+1.042\times10^6G_Q)^2$$

Rearranging terms

$$+1.09\times10^{12}G_Q^2+5.53\times10^6G_Q+6.09=0 \tag{95}$$

The positive root of this equation is approximately $+ 6.78 \times 10^{-7} \frac{ft}{lb\text{-}ft} = G_Q$ This value of G_Q is not unreasonably small when it is noted that the steady state shaft torque = 3.1×10^5 lb-ft.

Substituting the relevant positive value into equation (91) yields,

$$\omega_n = (2.88 + 1.042 \times 10^6 \times 6.78 \times 10^{-7}) \text{ sec}^{-1}$$

$$\omega_n = 2.17 \text{ sec}^{-1}$$

The $\frac{\omega'(s)}{V_o'(s)}$ is plotted in Figure E-6 for these values of G_Q and ω_n.

4. Thrust Sensing:

Propeller thrust can also be considered as a linear function of V_o, ω, and p just as Q_p.

$$T = K_4^* V_o + K_5^* p + K_6^* \tag{96}$$

where

$$K_4^* = \left.\frac{\partial T}{\partial V_o}\right| \text{ at the operating point} \tag{97}$$

$$K_5^* = \left.\frac{\partial T}{\partial p}\right| \text{at the operating point} \tag{98}$$

$$K_6^* = \left.\frac{\partial T}{\partial \omega}\right| \text{ at the operating point} \tag{99}$$

Values for K_4^*, K_5^*, and K_6^* are found exactly as were

values for previous stored variables. Again using Troost's curves:

$$K_4^* = \frac{\Delta T}{\Delta V_o} = \frac{K_T \rho n^2 D^4}{(.2)nD} = \frac{(-.04)(1.024)(\frac{10}{6})^2(18.25)^4}{(.2)(\frac{10}{6})(18.25)}$$

$$K_4^* = -1.325 \times 10^3 \ \frac{\text{lb-sec}}{\text{ft}} ,$$

$$K_5^* = \frac{\Delta T}{\Delta P} = \frac{K_T \rho n^2 D^4}{(.2)\frac{\rho}{D} D} = \frac{(08)(1.024)(\frac{10}{6})^2(18.25)^4}{(.2)(1.15)(18.25)}$$

$$K_5^* = 6.00 \times 10^3 \ \frac{\text{lb}}{\text{ft}} ,$$

and

$$K_6^* = \frac{\Delta T}{\Delta \omega} = \frac{K_T \rho n^2 D^4}{(.2)(n)(2\pi)} = \frac{(.04)(1.024)(\frac{10}{6})^2(18.25)^4}{(.2)(\frac{10}{6})2\pi}$$

$$K_6^* = 2.47 \times 10^4 \ \frac{\text{lb-sec}}{\text{rad}} .$$

Incrementally, equation (96) becomes

$$T^1 = K_4^* V_o' + K_5^* p' + K_6^* \quad , \tag{100}$$

The block diagram for the system sensing thrust is shown in Figure E-8.

In order to determine the effect on ω' of thrust sensing regulation it is necessary to add the paths that generated ω' from V_o', p', and Q_p'. This is shown in Figure E-9.

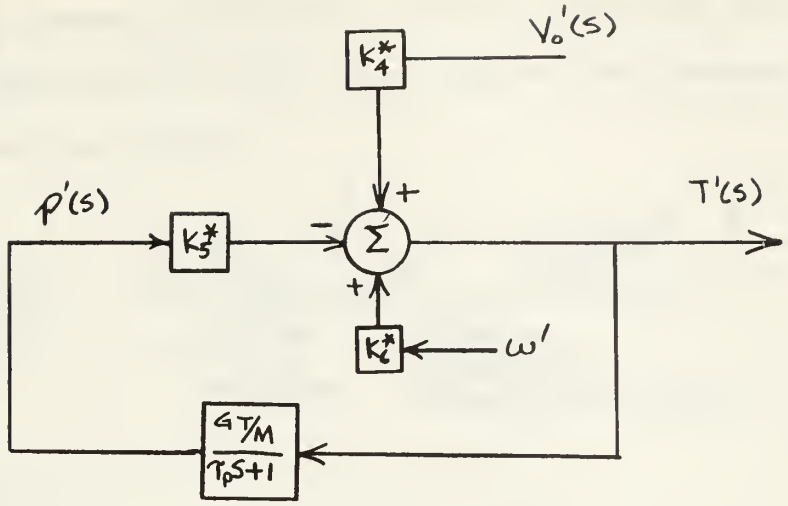

FIGURE E-8

System With Thrust Sensing

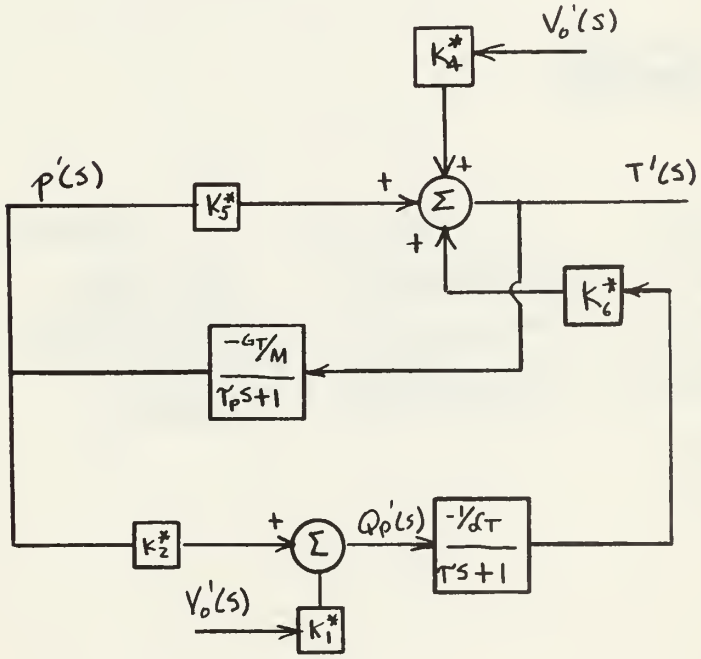

FIGURE E-9

Block Diagram of Complete Thrust Sensing Regulation Showing Generation of

The transfer function between $V_o'(s)$ and $\omega'(s)$ is more complicated in this case due to the presence of two paths and two loops.

$$\frac{\omega'(s)}{V_o'(s)} = \frac{-\left(\frac{1/\alpha_T}{1+\tau s}\right)\left[K_1^* + \frac{K_4^* G_T K_2^*}{(\tau_p s+1)}\right]}{1 + \frac{K_5^* G_T}{M(\tau_p s+1)} - \frac{K_6^* K_2^* G_T}{M\alpha_T(\tau_p s+1)(\tau s+1)}} \qquad (101)$$

Rearranging:

$$\frac{\omega'(s)}{V_o'(s)} = \frac{-\frac{K_1^*}{\tau\alpha_T}s - \left(\frac{K_1^*}{\alpha_T\tau\tau_p} + \frac{K_2^* K_4^* G_T}{\alpha_T\tau\tau_p M}\right)}{s^2 + \left(\frac{2\tau + 2\tau_p}{\tau_p\tau} + \frac{K_5^* G_T}{M\tau_p}\right)s + \left(\frac{1}{\tau\tau_p} + \frac{K_5^* G_T}{M\tau\tau_p} - \frac{K_6^* K_2^* G_T}{M\alpha_T\tau\tau_p}\right)} \qquad (102)$$

Substituting Values:

$$\frac{\omega'(s)}{V_o'(s)} = \frac{\frac{6610}{(3.28)(10.62)10^4}s - \left\{\frac{-6610}{10.62\times10^4\times3.28\times.56} + \frac{2.96\times10^4(-1.325\times10^3)G_T}{(10.62)(3.28)(.56)(.063)10^4}\right\}}{s^2 + \left\{\frac{2(3.28+.56}{(3.28)(.56)} + \frac{6\times10^3 G_T}{(.063)(.56)}\right\}s + \left\{\frac{1}{(3.28)(.56)} + \frac{6\times10^3 G_T}{(.063)(.56)(3.28)} - \frac{2.47\times10^4(2.96\times10^4)G_T}{(.063)(10.62)(10^4)(3.28)(.56)}\right\}}$$

$$\frac{\omega'(s)}{V_o'(s)} = \frac{.01895\ S - (-.0339 - 3190\ G_T)}{S^2+(2.09+1.7x10^5G_T)S + (0.545-7.6x10^3G_T)} \qquad (103)$$

Again setting $\zeta = 0.4$

$$2\zeta\omega_n = 2.09 + 1.7 \times 10^5\ G_T$$

$$\omega_n = 2.61 + 2.12 \times 10^5\ G_T$$

Solving for G_T:

$$(2.61 + 2.12 \times 10^5 G_T)^2 = (.545 - 7.6 \times 10^3 G_T)$$

$$4.5 \times 10^{10} G_T^2 + 4.31 \times 10^5 G_T + 5.26 = 0 \qquad (104)$$

Equation (104) has only imaginary roots. In fact setting $G_T=0$ in equation (103) results in

$$\omega_n = 0.736\ \text{sec}^{-1}$$

and $\zeta = 1.42$,

as well as a gain at zero frequency

$$\frac{\omega'(0)}{V'(0)} = -\ 0.0621\ ;\ 10 \log_{10} \left| \frac{\omega'(0)}{V'(0)} \right| = -12.06$$

which checks with the fixed pitch case as it must.

For all values of G_T greater than zero, ζ increases and zero frequency gain also increases.

For negative values of G_T, the pitch control mechanism would sense a decrease in thrust and respond by decreasing pitch which would further decrease thrust and the system would settle at zero pitch, zero thrust, and maximum ω .

Assuming a value of $G_T = +\ 10^{-5}\ \frac{ft}{lb}$, the unfortunate dilatorius effect of the thrust sensing can be shown.

Equation (103) becomes

$$\frac{\omega'(s)}{V_o'(s)} = \frac{+.018955 + .0658}{S^2 + 3.79\ S + (.469)} \qquad (105)$$

Equation (105) is plotted in Figure E-6 for comparison purposes.

APPENDIX F

References

A. Books

1. Bigelow, H.B. and W.T. Edmondson. Wind Waves at Sea, Breakers and Surf. Hydrographic Office Publication No. 602. Washington: U.S. Government Printing Office, 1947.

2. Rossell, Henry E. and Lawrence B. Chapman. Principles of Naval Architecture, Vol II. New York: Society of Naval Architects and Marine Engineers, 1941.

3. Ahrendt, William R. Servomechanism Practice. New York: McGraw-Hill Book Co. Inc., 1954.

4. MacMillan, R.H. An Introduction to the Theory of Control in Mechanical Engineering. Cambridge: Cambridge University Press, 1951.

5. Pinkus, Oscar and Beno Sternlicht. Theory of Hydrodynamic Lubrication. New York: McGraw-Hill Book Co., 1961.

6. Shaw, Milton C. and E. Fred Macks. Analysis and Lubrication of Bearings. New York: McGraw-Hill Book Co., 1949.

7. Gibson, John E. and Franz B. Tuteur. Control Systems Engineering. New York: McGraw-Hill Book Co., 1958.

8. Marks, Lionel S. (Editor). Mechanical Engineers Handbook 4th Edition. New York: McGraw-Hill Book Co. 1941.

9. Truxal, John G. Control Engineers Handbook. New York: McGraw-Hill Book Co., 1958.

10. Seward, Herbert Lee. Marine Engineering Vol II. New York: Society of Naval Architects and Marine Engineers, 1944.

11. Rupp, Lewis A. "Controllable Pitch Propellers," Transactions of the Society of Naval Architects and Marine Engineers, 56: 272-438, 1948.

12. Johnson, Charles H. "A Marine Gas Turbine Installation," New York Metropolitan Section of the Society of Naval Architects and Marine Engineers Paper, March 22, 1946.

13. Ruge, Arthur C. "The Bonded Wire Gage Torquemeter," Proceedings of the Society for Experimental Stress Analysis, Vol I, No. 2, 1943.

14. Panagopulos, E. "Design-Stage Calculations of Torsional, Axial and Lateral Vibrations of Marine Shafting," Society of Naval Architects and Marine Engineers Paper, Nov. 1950.

15. Powell, S. Curtis and W.V. Bassett, "Practical Aspects of Torsional Vibration in Marine Geared-Turbine Propulsion Units," Socity of Naval Architects and Marine Engineers Paper, March 1944.

16. Sutton, A.D. "Torsional Vibration of a Geared Turbine Propulsion System," New England Section of the Society of Naval Architects and Marine Engineers Paper, October 1953.

17. Lewis, F.M. "Propeller Coefficients and the Powering of Ships," Society of Naval Architects and Marine Engineers Paper, Nov. 1951.

18. Lewis, F.M. andJ. Auslaender. "Virtual Inertia of Propellers," Propeller Tunnel Report, Department of Naval Architecture and Marine Engineering, Massachusetts Institute of Technology, March 1960.

19. Poritsky H. and C.S.L. Robinson. "Torsional Vibration in Geared-Turbine Propulsion Equipment," Journal of Applied Mechanics, 62: A-117, September 1940.

20. Troost, Laurens. "A Simplified Method for Preliminary Powering of Single Screw Merchant Ships," New England Section of the Society of Naval Architects and Marine Engineers Paper, October 1955.

C. Periodical and Reports

21. Odden, C.R. "LST-1156-Class Controllable Pitch Propeller Maintenance, Hydralic Servo-System," Bureau of Ships Journal, p. 18, January 1961.

22. Morgan, William B. "Open Water Test Series of a Controllable Pitch Propeller with Varying Number of Blades," David Taylor Model Basin Report No. 932, November 1954.

23. McCarthy, J.H., N.H. Norley, and G.L. Ober, "The Performance of a Fully Submerged Propeller in Regular Waves," David Taylor Model Basin Report No. 1440, May 1961.

24. Boswell, Robert J. "A Method of Calculating the Spindle Torque of a Controllable-Pitch Propeller at Design Conditions," David Taylor Model Basin Report No. 1529, August 1961.

25. Bates, James L. "The Victory Ship Design," Marine Engineering and Shipping Review XLIX, No.4:154, April 1944.

26. Oilgear Co. Data Sheet on Fluid Power Pumps and Motors. Type DH-1100 psi.

D. Theses

27. Payne, Herbert. Analytical Methods of Determining the Speed Response Characteristics of Engine-Propeller Systems. Electrical Engineering Department Masters Thesis; M.I.T., 1946.

28. Brown, Neal Alvin. Determination of the Steady State Hydrodynamic Forces and Moment Acting on Propeller Blades. Naval Architecture and Marine Engineering Department Masters Thesis, M.I.T., 1959.

29. Chen, Yu Shu and Tzu Y Chu. Design of the Controllable-Pitch Propeller by Tunnel Test. Naval Architecture and Marine Engineering Department Masters Thesis, M.I.T., 1946.

30. Price, Ira Robert. Effect of Entrained Water on Virtual Inertia of Ship Propellers. Naval Architecture and Marine Engineering Thesis, M.I.T. 1953.

31. Moisan, Carol S. Moment of Inertia of Marine Propellers. Naval Architecture and Marine Engineering Thesis, M.I.T., 1953.

32. O'Connell, John D. and Evenson M. Burtis. Measurement of Ship Model Wake Variation in Rough Water. Naval Architecture and Marine Engineering Thesis, M.I.T., 1960.